Quasi-interpolating bivariate dual $\sqrt{2}$-subdivision using 1D stencils

Lincong Fang * Bin Han † Yi Shen‡

Abstract

In this paper, we study bivariate dual $\sqrt{2}$-subdivision schemes using one-dimensional (1D) stencils and reproducing bivariate polynomials of high orders. We show that such dual $\sqrt{2}$-subdivision schemes always possess the quasi-interpolating property (*i.e.,* they interpolate bivariate polynomials of high orders) and are intrinsically linked to both 1D primal interpolating subdivision schemes and 1D masks having linear-phase moments. Using only 1D stencils, such subdivision schemes can be straightforwardly implemented on any quadrilateral meshes and there is no need to design special subdivision rules near extraordinary or boundary vertices. In this paper, we concentrate on a particular quasi-interpolating dual $\sqrt{2}$-subdivision scheme using 4-point 1D stencils and interpolating all bivariate cubic polynomials. This dual $\sqrt{2}$-subdivision scheme has C^2 smoothness near any ordinary vertex guaranteed by the smoothness of its underlying basis/refinable function, while it achieves C^1 smoothness near an extraordinary vertex by our numerical calculation using the known technique of analyzing characteristic maps. As an illustration, we apply the proposed dual $\sqrt{2}$-subdivision scheme to several arbitrary polyhedra meshes to demonstrate the generated subdivision surfaces.

Keywords: surface modeling; $\sqrt{2}$-subdivision; quasi-interpolating property; dual scheme; linear-phase moments; refinable function.

1 Introduction

Subdivision schemes have been one of the most popular tools for the free-form surface modeling in computer graphics. For an initial control mesh of arbitrary topology, we will get a sequence of finer and finer meshes, and finally a limiting surface. The faces of such surface mesh are usually regular polygons, such as quadrilaterals, triangles, or hexagons. Numerous subdivision schemes have been studied and the schemes can be performed by either face split or vertex split. The schemes using face split are called primal, and the schemes using vertex split are called dual. The Catmull-Clark subdivision [1] is an example of primal, while the Doo-Sabin subdivision [4] is an example of dual.

Primal schemes can be interpolating or approximating. For primal schemes, vertices of the coarser mesh are retained, and a new vertex is inserted on each edge and for each face. New faces are created for each old face, one for each vertex adjacent to it. The vertices from the previous level are called even vertices, while the newly created vertices are called odd vertices. If each even vertex has the same geometric position for different subdivision levels, the scheme is interpolating, otherwise, it is approximating. Interpolation is an attractive feature for geometric modeling, however, the quality of these surfaces is usually lower than the quality of surfaces produced by approximating schemes.

For dual schemes, new vertices are created for each old vertex, one for each face adjacent to it. A new face is created for each vertex and each edge, while old faces are retained. Consequently, a dual scheme cannot possess the interpolation property. For a quadrilateral mesh, if a dual scheme is performed, then the valence of each vertex is 4 in the new mesh.

Various subdivision schemes are named according to the number of vertices from the current level to the next. For example, a scheme is called a $\sqrt{2}$-subdivision [14, 20, 21, 18, 27] if the number of vertices is roughly doubled, so as to $\sqrt{3}$-subdivision [17, 19, 23], $\sqrt{5}$-subdivision [16], and $\sqrt{7}$-subdivision [2]. In computer graphics, two consecutive steps of a $\sqrt{2}$-subdivision scheme are equivalent to one 1-to-4 split subdivision. Accordingly, there are two families of $\sqrt{2}$-subdivision schemes, being named the primal and the dual $\sqrt{2}$-subdivision schemes. Notice that $\sqrt{2}$-subdivision will produce more resolution levels in order to achieve a smoother transition between different resolution levels for level-of-detail modeling. This feature of $\sqrt{2}$-subdivision schemes is desired for some applications in computer aided geometric design (CAGD).

*L. Fang is with the School of Information Management and Artificial Intelligence, Zhejiang University of Finance and Economics, Hangzhou, China 310018. Email: lincongfang@gmail.com

†B. Han is with the Department of Mathematical and Statistical Sciences, University of Alberta, Edmonton, Canada, T6G 2G1. Email: bhan@ualberta.ca

‡Y. Shen is with the Department of Mathematics, Zhejiang Sci-Tech University, Hangzhou, China, 310018. E-mail: yshen@zstu.edu.cn

This paper is motivated by the work [15] on constructing quincunx tight wavelet frames having high vanishing moments. Let $M_{\sqrt{2}}$ be the following 2×2 integer matrix

$$M_{\sqrt{2}} := \begin{bmatrix} 1 & 1 \\ 1 & -1 \end{bmatrix}. \tag{1.1}$$

Note that the two eigenvalues $\pm\sqrt{2}$ of $M_{\sqrt{2}}$ are larger than one in modulus. Moreover,

$$M_{\sqrt{2}}\mathbb{Z}^2 = \{(k_1, k_2) \in \mathbb{Z}^2 \ : \ k_1 + k_2 \text{ is even}\},$$

which is often called the quincunx lattice in the literature. Consequently, the matrix $M_{\sqrt{2}}$ in (1.1) is called the quincunx dilation matrix in wavelet analysis and is often called the $\sqrt{2}$-dilation matrix in the literature of CAGD. Thus, a subdivision scheme using the dilation matrix $M_{\sqrt{2}}$ is called a $\sqrt{2}$-subdivision scheme and is naturally defined on quadrilateral meshes.

We observe that the bivariate masks $\boldsymbol{a}^{2D}_{2n,2n}$ with $n \in \mathbb{N}$ in [15, Theorem 2.1] have the following striking property: all the nonzero elements $\boldsymbol{a}^{2D}_{2n,2n}(k_1, k_2)$ for $(k_1, k_2) \in \mathbb{Z}^2$ only appear on two special straight lines $\{(k_1, k_1) \ : \ k_1 \in \mathbb{Z}\}$ and $\{(k_1, 1 - k_1) \ : \ k_1 \in \mathbb{Z}\}$. For example, the mask $\boldsymbol{a}^{2D}_{4,4}$ (denoted by $\boldsymbol{a}$ here) in [15, Theorem 2.1] is given by

$$\boldsymbol{a} = \begin{bmatrix} -\frac{1}{32} & 0 & 0 & -\frac{1}{32} \\ 0 & \frac{9}{32} & \frac{9}{32} & 0 \\ 0 & \boxed{\frac{9}{32}} & \frac{9}{32} & 0 \\ -\frac{1}{32} & 0 & 0 & -\frac{1}{32} \end{bmatrix}_{[-1,2]^2}, \tag{1.2}$$

where the boxed number is at the origin and the notation $[-1, 2]^2$ indicates the domain of $\boldsymbol{a}$, *i.e.,*

$$\boldsymbol{a}(0,0) = \boldsymbol{a}(1,0) = \boldsymbol{a}(0,1) = \boldsymbol{a}(1,1) = \frac{9}{32}$$

and

$$\boldsymbol{a}(-1,-1) = \boldsymbol{a}(-1,2) = \boldsymbol{a}(2,2) = \boldsymbol{a}(2,-1) = -\frac{1}{32}.$$

Hence, its associated two stencils $\{2\boldsymbol{a}(k_1, k_2) \ : \ k_1, k_2 \in \mathbb{Z} \text{ with even } k_1+k_2\}$ and $\{2\boldsymbol{a}(k_1, k_2) \ : \ k_1, k_2 \in \mathbb{Z} \text{ with odd } k_1+k_2\}$ are essentially 1D stencils, which are the same due to the symmetry of the mask $\boldsymbol{a}$ and are given in Figure 1.

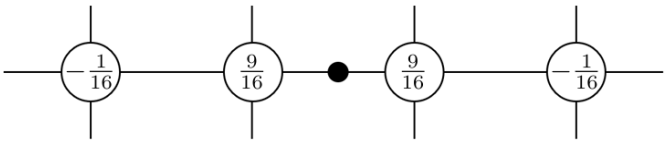

Figure 1: The even stencil $\{2\boldsymbol{a}(k_1, k_2) \ : \ k_1, k_2 \in \mathbb{Z} \text{ with even } k_1 + k_2\}$ and the odd stencil $\{2\boldsymbol{a}(k_1, k_2) \ : \ k_1, k_2 \in \mathbb{Z} \text{ with odd } k_1 + k_2\}$ are the same 1D stencils. It is the 4-point 1D stencil that can reproduce cubic polynomials.

Hence, the 2D stencil in Figure 1 is essentially a 1D stencil for the $\sqrt{2}$-subdivision scheme. Using 1D stencils for bivariate $\sqrt{2}$-subdivision schemes offers certain advantages in CAGD. For example, the $\sqrt{2}$-subdivision scheme using the 1D stencil in Figure 1 can be straightforwardly implemented for any quadrilateral meshes and there is no need to design special subdivision rules near extraordinary or boundary vertices. Departing from the viewpoint of quincunx tight wavelet frames in [15], in this paper we are motivated by the above discussions to study bivariate dual $\sqrt{2}$-subdivision schemes using essentially 1D stencils and reproducing bivariate polynomials of high orders from the perspective of CAGD. More precisely, for any given finitely supported 1D mask $\boldsymbol{a}^{1D} = \{\boldsymbol{a}^{1D}(k)\}_{k\in\mathbb{Z}}$, we shall study the following special two-dimensional (2D) mask $\boldsymbol{a}^{2D}$:

$$\boldsymbol{a}^{2D}(k_1, k_2) := \begin{cases} \frac{1}{2}\boldsymbol{a}^{1D}(k_1) & \text{if } k_2 = k_1 \ \text{ or } \ k_2 = 1 - k_1, \\ 0, & \text{otherwise,} \end{cases} \qquad \text{for all } k_1, k_2 \in \mathbb{Z}. \tag{1.3}$$

Because the smoothness of the underlying basis/refinable function is known to be closely linked to the polynomial reproducing property, in Section 2, we shall investigate the connections between the polynomial reproducing property of the special 2D mask $\boldsymbol{a}^{2D}$ in (1.3) and the property of the 1D mask $\boldsymbol{a}^{1D}$.

In this paper, we shall concentrate on the dual $\sqrt{2}$-subdivision scheme given by the mask $\boldsymbol{a}$ in (1.2), which can handle arbitrary quadrilateral meshes and which enjoys the quasi-interpolating property (*i.e.,* the interpolation property on bivariate polynomials of certain degrees). The associated subdivision rule is easy to be implemented, and no particular rules are needed to handle extraordinary vertices or irregular faces. The limit surface possess C^2-continuity except for some extraordinary points. Particularly, the proposed scheme can exactly reconstruct bivariate polynomial surfaces of high orders. After two consecutive subdivisions, the proposed dual $\sqrt{2}$-subdivision usually yields a mesh with the same topology structure as that generated by one step of the Doo-Sabin subdivision.

The rest of the paper is organized as follows. Section 2 gives some theoretical analysis of the proposed subdivision scheme. Section 3 introduces the subdivision rules of the proposed $\sqrt{2}$-subdivision and discusses the smoothness near extraordinary vertices. Section 4 shows the experimental results of the proposed scheme. Finally, Section 5 gives a short conclusion.

2 Bivariate dual $\sqrt{2}$-subdivision schemes using 1D stencils

In this section, we shall study $\sqrt{2}$-subdivision schemes using 1D stencils through the special construction in (1.3). To do so, we need to recall some necessary background and definitions.

2.1 Background and necessary definitions

The study on refinable functions in wavelet theory provides theoretical analysis at ordinary vertices for convergence and smoothness of subdivision schemes, including existing classical schemes. Moreover, a subdivision scheme can be considered as the discrete version of a cascade algorithm [13, 8]. Because we have to consider subdivision schemes and refinable functions in both dimension one and two, let us recall several definitions in a general d dimension. A $d \times d$ integer matrix M is called a dilation matrix if all the eigenvalues of M are greater than one in modulus. Later on, we are particularly interested in the dilation factor $M = 2$ for $d = 1$, and the particular dilation matrix $M = M_{\sqrt{2}}$ in (1.1) for $d = 2$. For the convenience of the reader, we shall explicitly state several notions for the particular dilation matrix $M_{\sqrt{2}}$. By $l_0(\mathbb{Z}^d)$ we denote all finitely supported sequences $\boldsymbol{u} = \{\boldsymbol{u}(\boldsymbol{k})\}_{\boldsymbol{k}\in\mathbb{Z}^d} : \mathbb{Z}^d \to \mathbb{R}$. Let $\boldsymbol{a} = \{\boldsymbol{a}(\boldsymbol{k})\}_{\boldsymbol{k}\in\mathbb{Z}^d} \in l_0(\mathbb{Z}^d)$ be a mask of a refinable function. For any sequence $\boldsymbol{v} = \{\boldsymbol{v}(\boldsymbol{k})\}_{\boldsymbol{k}\in\mathbb{Z}^d} : \mathbb{Z}^d \to \mathbb{R}$, the subdivision operator $S_{\boldsymbol{a},M}$ is defined to be (e.g., see [8, (7.1.1)])

$$[S_{\boldsymbol{a},M}\boldsymbol{v}](\boldsymbol{n}) := |\det(M)| \sum_{\boldsymbol{k}\in\mathbb{Z}^d} \boldsymbol{a}(\boldsymbol{n} - M\boldsymbol{k})\boldsymbol{v}(\boldsymbol{k}), \quad \boldsymbol{n} \in \mathbb{Z}^d. \tag{2.1}$$

A primal subdivision scheme puts the subdivided data $[S^j_{\boldsymbol{a},M}\boldsymbol{v}](\boldsymbol{n})$ at the position $M^{-j}\boldsymbol{n}$. Different to a primal subdivision scheme, a dual subdivision scheme puts the subdivision data $[S^j_{\boldsymbol{a},M}\boldsymbol{v}](\boldsymbol{n})$ at the position $M^{-j}(\boldsymbol{n} + \boldsymbol{c}_{\boldsymbol{a}})$, where $\boldsymbol{c}_{\boldsymbol{a}} \in \mathbb{R}^d$ is a compatible nonzero shift. For example, for a dual $\sqrt{2}$-subdivision scheme using the dilation matrix $M_{\sqrt{2}}$ in (1.1), the shift is $\boldsymbol{c}_{\boldsymbol{a}} = (1/2, 1/2)$. For a compactly supported function $\phi \in L_2(\mathbb{R}^d)$, if it satisfies the refinement equation

$$\phi = |\det(M)| \sum_{\boldsymbol{k}\in\mathbb{Z}^d} \boldsymbol{a}(\boldsymbol{k})\phi(M \cdot -\boldsymbol{k}), \tag{2.2}$$

then ϕ is said to be the refinable function associated with the mask $\boldsymbol{a}$ if ϕ is normalized with $\int_{\mathbb{R}^d} \phi(\boldsymbol{x})d\boldsymbol{x} = 1$. In particular, if $\sum_{\boldsymbol{k}\in\mathbb{Z}^d} \boldsymbol{a}(\boldsymbol{k}) = 1$, then its associated refinable/basis function ϕ is often determined through its Fourier transform $\hat{\phi}(\boldsymbol{\omega}) := \int_{\mathbb{R}^d} \phi(\boldsymbol{x})e^{-i\boldsymbol{\omega}\cdot\boldsymbol{x}}d\boldsymbol{x}$ by

$$\hat{\phi}(\boldsymbol{\omega}) = \prod_{j=1}^{\infty} \hat{\boldsymbol{a}}((M^T)^{-j}\boldsymbol{\omega})$$

for $\boldsymbol{\omega} \in \mathbb{R}^d$, where $\hat{\boldsymbol{a}}(\boldsymbol{\omega}) := \sum_{\boldsymbol{k}\in\mathbb{Z}^d} \boldsymbol{a}(\boldsymbol{k})e^{-\mathbf{i}\boldsymbol{k}\cdot\boldsymbol{\omega}}$ is a $2\pi\mathbb{Z}^d$-periodic d-variate trigonometric polynomial.

It is well known that the smoothness of a refinable function is closely linked to the sum rules of its underlying mask (*i.e.,* [13, 8, 9]). Define $\mathbb{N}_0 := \mathbb{N} \cup \{0\}$. For $\boldsymbol{\mu} = (\mu_1, \ldots, \mu_d)^T \in \mathbb{N}_0^d$ and $\boldsymbol{x} = (x_1, \ldots, x_d)^T \in \mathbb{R}^d$, we define $|\boldsymbol{\mu}| := \mu_1 + \cdots + \mu_d$ and $\boldsymbol{x}^{\boldsymbol{\mu}} := x_1^{\mu_1} \cdots x_d^{\mu_d}$. A finitely supported mask $\boldsymbol{a} \in l_0(\mathbb{Z}^d)$ has *order m sum rules with respect to M* if

$$\sum_{\boldsymbol{k}\in\mathbb{Z}^d} \boldsymbol{a}(\boldsymbol{\gamma} + M\boldsymbol{k})(\boldsymbol{\gamma} + M\boldsymbol{k})^{\boldsymbol{\mu}} = \sum_{\boldsymbol{k}\in\mathbb{Z}^d} \boldsymbol{a}(M\boldsymbol{k})(M\boldsymbol{k})^{\boldsymbol{\mu}}, \qquad \forall\ \boldsymbol{\mu} \in \mathbb{N}_0^d,\ |\boldsymbol{\mu}| < m,\ \boldsymbol{\gamma} \in \Gamma_M := [M[0,1)^d] \cap \mathbb{Z}^d. \tag{2.3}$$

We define $\mathrm{sr}(\boldsymbol{a}, M) := m$ to be the largest such integer m. By $\mathbb{P}_{m-1}$ we denote the set of all d-variate polynomials of total degree less than m. It is well known ([9, Theorem 3.5]) that a mask $\boldsymbol{a}$ has order m sum rules with respect

to the dilation matrix M if and only if $S_{\boldsymbol{a},M}\mathbb{P}_{m-1} \subseteq \mathbb{P}_{m-1}$, that is, the subdivision operator $S_{\boldsymbol{a},M}$ can reproduce all polynomials of degree less than m. For $d = 1$ and $M = 2$, we have $\Gamma_2 = \{0, 1\}$ and a mask $\boldsymbol{a} \in l_0(\mathbb{Z})$ has order m sum rules with respect to the dilation factor 2 if and only if

$$\sum_{k\in\mathbb{Z}} \boldsymbol{a}(1+2k)(1+2k)^j = \sum_{k\in\mathbb{Z}} \boldsymbol{a}(2k)(2k)^j, \qquad \forall\, j = 0, \ldots, m-1. \tag{2.4}$$

A 1D mask $\boldsymbol{a} \in l_0(\mathbb{Z})$ is called *an interpolating mask* with respect to the dilation factor 2 if $\boldsymbol{a}(2k) = 0$ for all $k \in \mathbb{Z}\backslash\{0\}$.

For $d = 2$ and $M = M_{\sqrt{2}}$ in (1.1), we have $\Gamma_{M_{\sqrt{2}}} = \{(0,0)^T, (1,0)^T\}$ and hence, a mask $\boldsymbol{a} \in l_0(\mathbb{Z}^2)$ has order m sum rules with respect to the dilation matrix $M_{\sqrt{2}}$ if and only if

$$\sum_{\boldsymbol{k}\in[(1,0)^T+M_{\sqrt{2}}\mathbb{Z}^2]} \boldsymbol{a}(\boldsymbol{k})\boldsymbol{k}^{\boldsymbol{\mu}} = \sum_{\boldsymbol{k}\in[M_{\sqrt{2}}\mathbb{Z}^2]} \boldsymbol{a}(\boldsymbol{k})\boldsymbol{k}^{\boldsymbol{\mu}}, \qquad \forall\ \boldsymbol{\mu} \in \mathbb{N}_0^2,\ |\boldsymbol{\mu}| < m. \tag{2.5}$$

Note that $M_{\sqrt{2}}\mathbb{Z}^2 = \{(k_1, k_2)^T \in \mathbb{Z}^2 \ :\ k_1 + k_2 \text{ is even}\}$ and $(1,0)^T + M_{\sqrt{2}}\mathbb{Z}^2 = \{(k_1, k_2)^T \in \mathbb{Z}^2 \ :\ k_1 + k_2 \text{ is odd}\}$. As discussed in [15, 8], to construct tight wavelet frames with high vanishing moments from a mask $\boldsymbol{a} \in l_0(\mathbb{Z}^d)$, it is necessary that the mask $\boldsymbol{a}$ must have high orders of both sum rules and linear-phase moments. We say that $\boldsymbol{a} \in l_0(\mathbb{Z}^d)$ has *order n linear-phase moments with phase* $\boldsymbol{c} \in \mathbb{R}^d$ if

$$\hat{\boldsymbol{a}}(\boldsymbol{\omega}) = e^{-\mathbf{i}\boldsymbol{c}\cdot\boldsymbol{\omega}} + O(\|\boldsymbol{\omega}\|^n), \qquad \boldsymbol{\omega} \to 0. \tag{2.6}$$

The largest such integer n is defined by $\mathrm{lpm}(\boldsymbol{a}) := n$. It is straightforward to observe from the definition of $\hat{\boldsymbol{a}}(\boldsymbol{\omega})$ that

$$\hat{\boldsymbol{a}}^{(\boldsymbol{\mu})}(0) = (-\mathbf{i})^{|\boldsymbol{\mu}|} \sum_{\boldsymbol{k}\in\mathbb{Z}^d} \boldsymbol{a}(\boldsymbol{k})\boldsymbol{k}^{\boldsymbol{\mu}}$$

for all $\boldsymbol{\mu} \in \mathbb{N}_0^d$. Consequently, the condition in (2.6) for order n linear-phase moments with phase $\boldsymbol{c} \in \mathbb{R}^d$ is just equivalent to

$$\sum_{\boldsymbol{k}\in\mathbb{Z}^d} \boldsymbol{a}(\boldsymbol{k})\boldsymbol{k}^{\boldsymbol{\mu}} = \boldsymbol{c}^{\boldsymbol{\mu}}, \qquad \text{for all } \boldsymbol{\mu} \in \mathbb{N}_0,\ |\boldsymbol{\mu}| < n. \tag{2.7}$$

In fact, it is well known in the literature of wavelet analysis ([9, Proposition 5.3]) that any tight wavelet frame derived from a mask $\boldsymbol{a} \in l_0(\mathbb{Z}^d)$, such that $\boldsymbol{a}$ is symmetric about a point, can have vanishing moments of order exactly $\min(\mathrm{sr}(\boldsymbol{a}, M), \frac{1}{2}\,\mathrm{lpm}(\boldsymbol{a}))$. This is the main reason that the masks constructed in [15, Theorem 2.1] must have high orders of both sum rules and linear-phase moments in advance. For more discussions on importance of linear-phase moments for orthogonal wavelets and tight wavelet frames with vanishing moments, see [9, 15, 10, 5]. However, the notion of linear-phase moments is much less known in CAGD. In this section, we shall show that the notion of linear-phase moments indeed plays a key role for constructing 2D masks $\boldsymbol{a}^{2D}$ in (1.3) from 1D masks $\boldsymbol{a}^{1D}$.

2.2 Main result on bivariate dual $\sqrt{2}$-subdivision using 1D stencils

We are now ready to study the relation between a given 1D mask $\boldsymbol{a}^{1D} \in l_0(\mathbb{Z})$ and its derived $2D$ mask $\boldsymbol{a}^{2D}$ defined in (1.3). For improved readability, the proof of the following result will be given in Appendix.

Theorem 2.1. *Let $\boldsymbol{a}^{1D} = \{\boldsymbol{a}^{1D}(k)\}_{k\in\mathbb{Z}} \in l_0(\mathbb{Z})$ be a finitely supported 1D mask such that $\sum_{k\in\mathbb{Z}} \boldsymbol{a}^{1D}(k) = 1$ (or equivalently, $\widehat{\boldsymbol{a}^{1D}}(0) = 1$). Define a finitely supported bivariate mask $\boldsymbol{a}^{2D}$ as in* (1.3)*. Then the following statements are equivalent to each other:*

(1) The bivariate mask $\boldsymbol{a}^{2D}$ has order m sum rules with respect to the dilation matrix $M_{\sqrt{2}}$ in (1.1)*.*

(2) The 1D mask $\boldsymbol{a}^{1D}$ has order m linear-phase moments with phase 1/2*,* i.e., *$\sum_{k\in\mathbb{Z}} \boldsymbol{a}^{1D}(k)k^j = 2^{-j}$ for all $j = 0, \ldots, m-1$.*

(3) The 1D interpolating mask $\boldsymbol{a}^I$ has order m sum rules with respect to the dilation factor 2*, where*

$$\boldsymbol{a}^I(k) := \begin{cases} \frac{1}{2}\boldsymbol{a}^{1D}(\frac{k-1}{2}), & \text{if } k \text{ is an odd integer,} \\ \frac{1}{2}, & \text{if } k = 0, \\ 0, & \text{otherwise,} \end{cases} \qquad k \in \mathbb{Z}. \tag{2.8}$$

Moreover, any of the above items (1)–(3) implies that the bivariate mask $\boldsymbol{a}^{2D}$ must have order m linear-phase moments with phase $(1/2,1/2)^T$, i.e.,

$$\sum_{\boldsymbol{k}\in\mathbb{Z}^2} \boldsymbol{a}^{2D}(\boldsymbol{k})\boldsymbol{k}^{\mu} = 2^{-|\mu|}, \quad \textit{for all} \quad \mu\in\mathbb{N}_0^2, \quad |\mu|<m. \tag{2.9}$$

Before making some remarks about Theorem 2.1, we present one example here with $m=4$ in Theorem 2.1. All 1D masks $\boldsymbol{a}^{1D}\in l_0(\mathbb{Z})$ with support $[-2,3]$, which are symmetric about the center $1/2$ and have order 4 linear-phase moments with phase $1/2$, must be given by

$$\boldsymbol{a} = \left\{2t, -\tfrac{1}{16}-6t, \boxed{\tfrac{9}{16}+4t}, \tfrac{9}{16}+4t, -\tfrac{1}{16}-6t, 2t\right\}_{[-2,3]},$$

where $t\in\mathbb{R}$ is a free parameter and the boxed number is at the origin. Hence, the associated interpolating mask $\boldsymbol{a}^I$ in (2.8) is given by

$$\boldsymbol{a}^I = \left\{t, 0, -\tfrac{1}{32}-3t, 0, \tfrac{9}{32}+2t, \boxed{\tfrac{1}{2}}, \tfrac{9}{32}+2t, 0, -\tfrac{1}{32}-3t, 0, t\right\}_{[-5,5]}.$$

By (1.3), the bivariate mask $\boldsymbol{a}^{2D}$ in Theorem 2.1 is given by

$$\boldsymbol{a}^{2D} = \begin{bmatrix} t & 0 & 0 & 0 & 0 & t \\ 0 & -\frac{1}{32}-3t & 0 & 0 & -\frac{1}{32}-3t & 0 \\ 0 & 0 & \frac{9}{32}+2t & \frac{9}{32}+2t & 0 & 0 \\ 0 & 0 & \boxed{\frac{9}{32}+2t} & \frac{9}{32}+2t & 0 & 0 \\ 0 & -\frac{1}{32}-3t & 0 & 0 & -\frac{1}{32}-3t & 0 \\ t & 0 & 0 & 0 & 0 & t \end{bmatrix}_{[-2,3]^2}. \tag{2.10}$$

For $t\neq\frac{3}{512}$, we have $\mathrm{lpm}(\boldsymbol{a}^{1D})=\mathrm{lpm}(\boldsymbol{a}^I)=\mathrm{lpm}(\boldsymbol{a}^{2D})=4$ and $\mathrm{sr}(\boldsymbol{a}^{2D},M_{\sqrt{2}})=\mathrm{sr}(\boldsymbol{a}^I,2)=4$. For $t=\frac{3}{512}$, we have $\mathrm{lpm}(\boldsymbol{a}^{1D})=\mathrm{lpm}(\boldsymbol{a}^I)=\mathrm{lpm}(\boldsymbol{a}^{2D})=6$ and $\mathrm{sr}(\boldsymbol{a}^{2D},M_{\sqrt{2}})=\mathrm{sr}(\boldsymbol{a}^I,2)=6$. We shall analyze the smoothness of the refinable functions associated with the masks $\boldsymbol{a}^{2D}$ in (2.10) at the end of this section. Note that the mask in (1.2) is a special case of the above mask $\boldsymbol{a}^{2D}$ with $t=0$.

2.3 Quasi-interpolating property, linear-phase moments and symmetry

We now make some remarks about Theorem 2.1. First of all, Theorem 2.1 tells us that $\mathrm{sr}(\boldsymbol{a}^{2D},M_{\sqrt{2}})=\mathrm{lpm}(\boldsymbol{a}^{1D})$. Hence, the order of linear-phase moments of the 1D mask $\boldsymbol{a}^{1D}$ characterizes the order of sum rules of the 2D mask $\boldsymbol{a}^{2D}$ in (1.3) and therefore, characterizes the polynomial reproducing property of the $\sqrt{2}$-subdivision scheme using the mask $\boldsymbol{a}^{2D}$, according to our previous discussions on the order of sum rules and the polynomial reproducing property of the subdivision operator $S_{\boldsymbol{a}^{2D},M_{\sqrt{2}}}$. Second, we observe from the definition of $\boldsymbol{a}^I$ in (2.8) that $\boldsymbol{a}^{1D}(k)=2\boldsymbol{a}^I(1-2k)$ for all $k\in\mathbb{Z}$, that is, $\boldsymbol{a}^{1D}$ is simply the flipped odd stencil of the interpolatory mask $\boldsymbol{a}^I$ in item (3) of Theorem 2.1. Therefore, we can construct a special 2D mask $\boldsymbol{a}^{2D}$ in (1.3) from any 1D interpolatory mask $\boldsymbol{a}^I$ and $\mathrm{sr}(\boldsymbol{a}^{2D},M_{\sqrt{2}})=\mathrm{sr}(\boldsymbol{a}^I,2)$. If one takes $\boldsymbol{a}^I$ to be any interpolating masks in Deslauriers and Dubuc [3], it turns out that the 2D mask $\boldsymbol{a}^{2D}$ in Theorem 2.1 agrees with the constructed mask in [15, Theorem 2.1] for constructing tight wavelet frames with high vanishing moments. Hence, in this sense, Theorem 2.1 extends [15, Theorem 2.1] from the perspective of subdivision schemes. Moreover, Theorem 2.1 shows that $\mathrm{lpm}(\boldsymbol{a}^{1D})=\mathrm{lpm}(\boldsymbol{a}^{2D})$, that is, the special mask $\boldsymbol{a}^{2D}$ in (1.3) having order m sum rules with respect to $M_{\sqrt{2}}$ automatically forces the mask $\boldsymbol{a}^{2D}$ to have order m linear-phase moments, which leads to the quasi-interpolating property. On one hand, for any mask $\boldsymbol{a}\in l_0(\mathbb{Z}^d)$, by [9, Theorem 3.5], $\mathrm{sr}(\boldsymbol{a},M)=m$ if and only if $S_{\boldsymbol{a},M}\boldsymbol{p}\in\mathbb{P}_{m-1}$ for any polynomial $\boldsymbol{p}\in\mathbb{P}_{m-1}$. However, how the reproduced polynomial $S_{\boldsymbol{a},M}\boldsymbol{p}$ is linked to the original polynomial $\boldsymbol{p}$ is dominated by the moments $\partial^{\mu}\hat{\boldsymbol{a}}(0):=(-i)^{\mu}\sum_{\boldsymbol{k}\in\mathbb{Z}^d}\boldsymbol{a}(\boldsymbol{k})\boldsymbol{k}^{\mu}$ for $|\mu|<m$. More precisely, [9, (3.13) and Lemma 3.1] tells us that

$$S_{\boldsymbol{a},M}\boldsymbol{p} = \sum_{\mu\in\mathbb{N}_0^d}\frac{(-i)^{\mu}}{\mu!}\partial^{\mu}[\boldsymbol{p}(M^{-1}\cdot)]\partial^{\mu}\hat{\boldsymbol{a}}(0), \qquad \boldsymbol{p}\in\mathbb{P}_{m-1}.$$

In particular, it is known in [9, Proposition 5.1] that a mask $\boldsymbol{a}\in l_0(\mathbb{Z}^d)$ has order m sum rules with respect to M and $\boldsymbol{a}$ has order m linear-phase moments with phase $\boldsymbol{c}\in\mathbb{R}^d$ if and only if

$$[S_{\boldsymbol{a},M}\boldsymbol{p}](\boldsymbol{k}) = \boldsymbol{p}(M^{-1}(\boldsymbol{k}-\boldsymbol{c})), \quad \text{for all} \quad \boldsymbol{p}\in\mathbb{P}_{m-1}. \tag{2.11}$$

We call (2.11) *the quasi-interpolating property*. A mask $\boldsymbol{a} \in l_0(\mathbb{Z}^d)$ is said to be *interpolating with respect to* M if $\boldsymbol{a}(M\boldsymbol{k}) = 0$ for all $\boldsymbol{k} \in \mathbb{Z}^d \backslash \{0\}$. It is straightforward to deduce that if an interpolating mask $\boldsymbol{a}$ has order m sum rules with respect to M, then the quasi-interpolating property in (2.11) must hold true with $\boldsymbol{c} = 0$. Therefore, the quasi-interpolating property in (2.11) gives us a weaker notion of the interpolation property: the subdivision scheme interpolates on every polynomial in $\mathbb{P}_{m-1}$ though itself is not interpolating (in particular, any dual schemes cannot possess the interpolating property).

For the mask $\boldsymbol{a}$ in (1.2) and more generally, the mask in (2.10), according to Theorem 2.1, $\mathrm{sr}(\boldsymbol{a}, M_{\sqrt{2}}) = \mathrm{lpm}(\boldsymbol{a}) = 4$. Therefore, the dual $\sqrt{2}$-subdivision scheme using the quasi-interpolating mask $\boldsymbol{a}$ in (1.2) or (2.10) interpolates all bivariate polynomials of degree up to 3. More precisely,

$$[S_{\boldsymbol{a},M}\boldsymbol{v}](i,j) = \boldsymbol{v}(M^{-1}(i-1/2, j-1/2))$$

for all $(i,j) \in \mathbb{Z}^2$ and any polynomial sequence $\boldsymbol{v}$ of degree at most 3.

Generally, a surface or curve is modeled by a mesh through connecting neighboring points. However, a mesh often has no natural coordinate system at $\mathbb{Z}^d$. To overcome this problem, the discrete points in $\mathbb{Z}^d$ are connected. For dimension one, the points in $\mathbb{Z}$ can be naturally connected by joining k with $k+1$ through a line segment for every $k \in \mathbb{Z}$. For dimension two, there are two basic standard meshes: the quadrilateral mesh $\mathbb{Z}^2_Q$ by connecting neighboring points through horizontal or vertical line segments, and the triangular mesh $\mathbb{Z}^2$ by connecting neighboring points horizontally, vertically, or along with 45° degrees through line segments. Then any given initial control mesh in dimension three can be locally interpreted as $\boldsymbol{v} = \{\boldsymbol{v}(\boldsymbol{k}) = (v_1(\boldsymbol{k}), v_2(\boldsymbol{k}), v_3(\boldsymbol{k}))\}_{\boldsymbol{k}\in\mathbb{Z}^2_Q}$. That is, the connectivity of $\mathbb{Z}^2_Q$ induces the connectivity of the mesh $\boldsymbol{v}$, whose vertices are indexed by elements in $\mathbb{Z}^2_Q$. Now a subdivision scheme produces a limiting surface through the recursively refined meshes $\{([S^j_{\boldsymbol{a},M}v_1](\boldsymbol{k}), [S^j_{\boldsymbol{a},M}v_2](\boldsymbol{k}), [S^j_{\boldsymbol{a},M}v_3](\boldsymbol{k}))\}_{\boldsymbol{k}\in\mathbb{Z}^2_Q}$ as $j \to \infty$. More precisely, the limiting subdivision surface can be regarded as a parametric surface $(T_1(u,v), T_2(u,v), T_3(u,v))$ for $(u,v)^T \in \mathbb{R}^2$, where for $\ell = 1, 2, 3$,

$$T_\ell(u,v) := \lim_{j\to\infty} [S^j_{\boldsymbol{a},M}v_\ell](\boldsymbol{k}_j) \quad \text{under the condition } \lim_{j\to\infty} M^{-j}(\boldsymbol{k}_j - \boldsymbol{c}) = (u,v)^T \in \mathbb{R}^2.$$

Note that a primal subdivision scheme uses the shift $\boldsymbol{c} = (0,0)^T$. If a bivariate mask $\boldsymbol{a}^{2D}$ has order m sum rules with respect to the dilation matrix $M_{\sqrt{2}}$, then by Theorem 2.1, the bivariate mask $\boldsymbol{a}^{2D}$ must have order m linear-phase moments with phase $\boldsymbol{c} := (1/2, 1/2)^T$ and consequently, by the above discussion, we conclude that the limiting subdivision surface $(T_1(u,v), T_2(u,v), T_3(u,v))$ for $(u,v)^T \in \mathbb{R}^2$ must satisfy $T_1 = v_1, T_2 = v_2, T_3 = v_3$ if the initial control mesh $\{(v_1(\boldsymbol{k}), v_2(\boldsymbol{k}), v_3(\boldsymbol{k}))\}_{\boldsymbol{k}\in\mathbb{Z}^2_Q}$ is given by choosing $v_1, v_2, v_3 \in \mathbb{P}_{m-1}$. That is, the subdivision scheme using the mask $\boldsymbol{a}^{2D}$ in Theorem 2.1 interpolates and preserves the initial control mesh (v_1, v_2, v_3) for all $v_1, v_2, v_3 \in \mathbb{P}_{m-1}$.

Finally, we make a remark on the symmetry of the 2D mask $\boldsymbol{a}^{2D}$ in Theorem 2.1. Let G be a finite set of $d \times d$ integer matrices, such that $|\det(E)| = 1$ for every $E \in G$ and G forms a symmetry group on $\mathbb{Z}^d$ under the matrix multiplication. A subdivision triplet $(\boldsymbol{a}; M; G)$ is introduced to apply a subdivision scheme in computer graphics for generating smooth curves and surfaces ([8, 6]). In a subdivision triple $(\boldsymbol{a}; M; G)$, the dilation matrix M must be compatible with G (*i.e.,* $MEM^{-1} \in G$ for all $E \in G$) and the mask $\boldsymbol{a}$ must be *G-symmetric with center* $\boldsymbol{c} \in \mathbb{R}^d$:

$$\boldsymbol{a}(E(\boldsymbol{k} - \boldsymbol{c}) + \boldsymbol{c}) = \boldsymbol{a}(\boldsymbol{k}), \quad \text{for all} \quad \boldsymbol{k} \in \mathbb{Z}^d. \tag{2.12}$$

For a finitely supported mask $\boldsymbol{a}$ which is G-symmetric with center $\boldsymbol{c} \in \mathbb{R}^d$, let ϕ be its refinable function satisfying (2.2) with the dilation matrix M. Then ϕ must be G-symmetric with the center $c_\phi \in \mathbb{R}^d$ (e.g., see [9, Theorem 5.4] or [12, Theorem 2.2]):

$$\phi(E(\cdot - \boldsymbol{c}_\phi) + \boldsymbol{c}_\phi) = \phi, \qquad \text{for all } E \in G \quad \text{with} \quad \boldsymbol{c}_\phi := (M - I_d)^{-1}\boldsymbol{c}.$$

In addition, for any $d \times d$ integer matrix $N := EMF$ with $E, F \in G$, the matrix N must be a dilation matrix and we must have $\mathrm{sr}(\boldsymbol{a}, N) = \mathrm{sr}(\boldsymbol{a}, M)$ and $\phi^N = \phi(\cdot + (M - I_d)^{-1}\boldsymbol{c} - (N - I_d)^{-1}\boldsymbol{c})$, where ϕ^N satisfies the refinement equation in (2.2) but with M being replaced by N. See [9, Theorem 5.4] and [12, Theorem 2.2] for more details about the relations between the symmetry of a mask $\boldsymbol{a}$ and the symmetry property of its refinable/basis function ϕ.

Masks $\boldsymbol{a}$ used in subdivision schemes must have symmetry, largely because there are no natural coordinates for meshes in CAGD. One of the symmetry groups associated with the quadrilateral mesh $\mathbb{Z}^2_Q$ is

$$D_4 := \left\{ \pm \begin{bmatrix} 1 & 0 \\ 0 & 1 \end{bmatrix}, \pm \begin{bmatrix} 1 & 0 \\ 0 & -1 \end{bmatrix}, \pm \begin{bmatrix} 0 & 1 \\ 1 & 0 \end{bmatrix}, \pm \begin{bmatrix} 0 & 1 \\ -1 & 0 \end{bmatrix} \right\}. \tag{2.13}$$

It is easy to check that the matrix $M_{\sqrt{2}}$ in (1.1) is compatible with the symmetry group D_4 in (2.13). It is now easy to observe that the 2D mask $\boldsymbol{a}^{2D}$ in (2.10) is D_4-symmetric with center $(1/2, 1/2)$. Hence, $(\boldsymbol{a}^{2D}; M_{\sqrt{2}}; D_4)$ forms a

subdivision triple. It is obvious that general masks $\boldsymbol{a}^{2D}$ in Theorem 2.1 are D_4-symmetric with center $(1/2, 1/2)$ if and only if the 1D mask $\boldsymbol{a}^{1D}$ is symmetric about the point $1/2$ (or equivalently, the interpolating mask $\boldsymbol{a}^I$ in Theorem 2.1 is symmetric about the origin). As we discussed before, due to the D_4-symmetry of a bivariate mask a^{2D}, if the quincunx dilation matrix $M_{\sqrt{2}}$ in (1.1) is replaced be any other dilation matrix $N := EM_{\sqrt{2}}F$ for $E, F \in D_4$, then their corresponding $\sqrt{2}$-subdivision schemes are essentially the same and their associated basis functions ϕ have the identical properties. Moreover, the refinable function ϕ is D_4-symmetric with the center $\boldsymbol{c}_\phi := (1/2, -1/2)^T$ satisfying $\phi(E(\boldsymbol{x} - \boldsymbol{c}_\phi) + \boldsymbol{c}_\phi) = \phi(\boldsymbol{x})$ for all $x \in \mathbb{R}^2$ and $E \in D_4$.

2.4 Smoothness near ordinary vertices

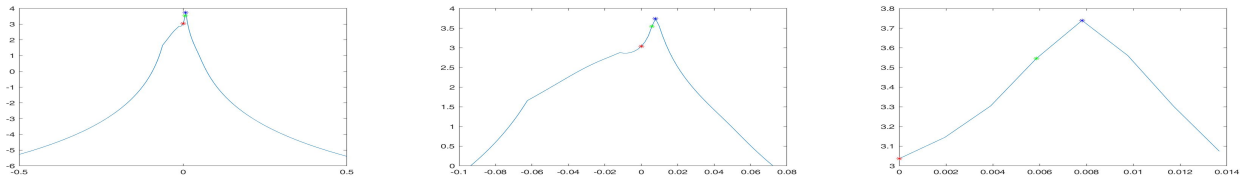

(a) $\mathrm{sm}_2(\boldsymbol{a}^{2D}, M_{\sqrt{2}})$ (b) $\mathrm{sm}_2(\boldsymbol{a}^{2D}, M_{\sqrt{2}}) > 0$ (c) $\mathrm{sm}_2(\boldsymbol{a}^{2D}, M_{\sqrt{2}}) > 3$

Figure 2: (a) is for the smoothness quantity $\mathrm{sm}_2(\boldsymbol{a}^{2D}, M_{\sqrt{2}})$ in (2.10) in Theorem 2.1 with $t \in [-0.5, 0.5]$. (b) is for the smoothness quantity $\mathrm{sm}_2(\boldsymbol{a}^{2D}, M_{\sqrt{2}}) > 0$ with $t \in [-0.0938, 0.0723]$. (c) is for the smoothness quantity $\mathrm{sm}_2(\boldsymbol{a}^{2D}, M_{\sqrt{2}}) > 3$ with $t \in [0, 0.0137]$ and their refinable functions $\phi \in C^2(\mathbb{R}^2)$. The red $*$ indicates the smoothness quantity $\mathrm{sm}_2(\boldsymbol{a}^{2D}, M_{\sqrt{2}}) \approx 3.03654$ at $t = 0$; The green $*$ indicates the smoothness quantity $\mathrm{sm}_2(\boldsymbol{a}^{2D}, M_{\sqrt{2}}) \approx 3.54575$ at $t = \frac{3}{512}$; The blue $*$ indicates the smoothness quantity $\mathrm{sm}_2(\boldsymbol{a}^{2D}, M_{\sqrt{2}}) \approx 3.73908$ at $t = \frac{1}{128}$.

To estimate the smoothness of the refinable function with respect to the dilation matrix defined in (1.1) and the masks defined in (1.2) or (2.10), we briefly recall the computation of the smoothness exponent defined in [13] (also see [8, Chapter 7]). More details on the smoothness exponent can be found in [13, 8, 15, 7] and many references therein. For $\boldsymbol{u} \in l_0(\mathbb{Z}^d)$ and $\boldsymbol{\mu} = (\mu_1, \ldots, \mu_d) \in \mathbb{N}_0^d$, we define

$$\nabla_{\boldsymbol{k}} \boldsymbol{u} := \boldsymbol{u} - \boldsymbol{u}(\cdot - \boldsymbol{k}), \quad \boldsymbol{k} \in \mathbb{Z}^d \qquad \text{and} \qquad \nabla^{\boldsymbol{\mu}} = \nabla_{\boldsymbol{e}_1}^{\mu_1} \cdots \nabla_{\boldsymbol{e}_d}^{\mu_d},$$

where $\boldsymbol{e}_j \in \mathbb{R}^d$ has only one nonzero entry which is one at the position jth coordinate. The Dirac sequence is denoted by δ such that $\delta(0) = 1$ and $\delta(\boldsymbol{k}) = 0$ for all $\boldsymbol{k} \in \mathbb{Z}^d \backslash \{0\}$. For a finitely supported mask $\boldsymbol{a} \in l_0(\mathbb{Z}^d)$ with $\hat{\boldsymbol{a}}(0) := \sum_{\boldsymbol{k} \in \mathbb{Z}^d} \boldsymbol{a}(\boldsymbol{k}) = 1$, the smoothness exponent $\mathrm{sm}_p(\boldsymbol{a}, M)$ is defined (*i.e.,* see [13, 7] and [8, (7.2.2)]) to be

$$\mathrm{sm}_p(\boldsymbol{a}, M) := \tfrac{d}{p} - \log_{\rho(M)} \rho(\boldsymbol{a}, M)_p, \qquad 1 \le p \le \infty,$$

where M is a $d \times d$ dilation matrix, $\rho(M)$ is the spectral radius of M, and

$$\rho(\boldsymbol{a}, M)_p := \sup \left\{ \lim_{n \to \infty} \|\nabla^{\boldsymbol{\mu}} S_{\boldsymbol{a}, M}^n \delta\|_{l_p(\mathbb{Z}^d)}^{1/n} : \ \boldsymbol{\mu} \in \mathbb{N}_0^d, \ |\boldsymbol{\mu}| = \mathrm{sr}(\boldsymbol{a}, M) \right\}.$$

It is well known that $\mathrm{sm}_\infty(\boldsymbol{a}, M) \ge \mathrm{sm}_2(\boldsymbol{a}, M) - d/2$. Taking the advantage of the symmetry property of masks and applying [7, Algorithm 2.1] to the mask $\boldsymbol{a}$ in (2.10) and the quincunx dilation matrix $M_{\sqrt{2}}$ in (1.1), we calculate the quantity $\mathrm{sm}_2(\boldsymbol{a}^{2D}, M_{\sqrt{2}})$ which is presented in Figure 2 for the parameter $t \in [-\frac{1}{2}, \frac{1}{2}]$. From Figure 2, we notice that the largest possible $\mathrm{sm}_2(\boldsymbol{a}^{2D}, M_{\sqrt{2}}) \approx 3.73908$ achieved at $t = \frac{1}{128}$ and hence $\mathrm{sm}_\infty(\boldsymbol{a}^{2D}, M_{\sqrt{2}}) \ge 2.73908$. For $t = \frac{3}{512}$, we have $\mathrm{sr}(\boldsymbol{a}^{2D}, M_{\sqrt{2}}) = 6 = \mathrm{lpm}(\boldsymbol{a}^{2D})$ and $\mathrm{sm}_2(\boldsymbol{a}^{2D}, M_{\sqrt{2}}) \approx 3.54575$; Hence $\mathrm{sm}_\infty(\boldsymbol{a}^{2D}, M_{\sqrt{2}}) \ge 2.54575$. For $t = 0$ (*i.e.,* the mask $\boldsymbol{a}$ in (1.2)), we have $\mathrm{sm}_2(\boldsymbol{a}^{2D}, M_{\sqrt{2}}) \approx 3.03654$ and hence $\mathrm{sm}_\infty(\boldsymbol{a}, M_{\sqrt{2}}) \ge 2.03654$. It follows from [8, Theorem 7.2.4] that $\phi \in C^2(\mathbb{R}^2)$. We conclude that the subdivision scheme (2.1) using the mask in (1.2) generates C^2-continuous limiting surfaces except at those extraordinary vertices. Hence, away from extraordinary vertices, the proposed subdivision scheme guarantees the continuity of the curvature of the generated surface. See Figures 3, 4, and 5 for the graphs of the refinable/basis functions and their partial derivatives associated with the masks $\boldsymbol{a}^{2D}$ in (2.10) with the parameters $t = 0, \frac{3}{512}$ and $\frac{1}{128}$. Our numerical illustration in Figure 5 seems to suggest that the refinable function ϕ associated the mask $\boldsymbol{a}^{2D}$ with $t = \frac{1}{128}$ probably belongs to $C^3(\mathbb{R}^2)$. However, beyond the estimate $\mathrm{sm}_\infty(\boldsymbol{a}^{2D}, M_{\sqrt{2}}) \ge \mathrm{sm}_2(\boldsymbol{a}^{2D}, M_{\sqrt{2}}) - 1 \approx 2.73908$, it is often a difficult task to accurately estimate the quantity $\mathrm{sm}_\infty(\boldsymbol{a}^{2D}, M_{\sqrt{2}})$ for the Hölder smoothness exponent. We leave this as a future research topic.

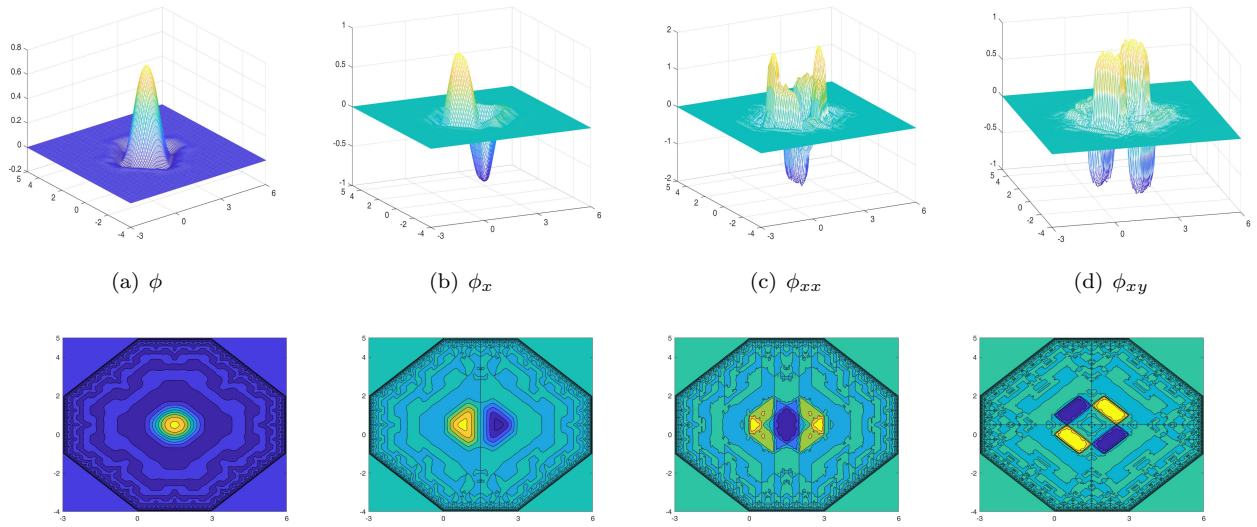

(a) ϕ (b) ϕ_x (c) ϕ_{xx} (d) ϕ_{xy}

(e) supp(ϕ) (f) supp(ϕ_x) (g) supp(ϕ_{xx}) (h) supp(ϕ_{xy})

Figure 3: (a)–(d) in the first row are respectively the refinable function ϕ (with the mask $\boldsymbol{a}^{2D}$ in (2.10) for $t = 0$), its first order partial derivative $\frac{\partial \phi}{\partial x}$, and its second order partial derivatives $\frac{\partial^2 \phi}{\partial x^2}$ and $\frac{\partial^2 \phi}{\partial x \partial y}$. (e)–(h) in the second row are their corresponding contours. Note that $\mathrm{sr}(\boldsymbol{a}^{2D}, M_{\sqrt{2}}) = \mathrm{lpm}(\boldsymbol{a}^{2D}) = 4$, $\mathrm{sm}_2(\boldsymbol{a}^{2D}, M_{\sqrt{2}}) \approx 3.03654$ for mask $\boldsymbol{a}^{2D}$ with $t = 0$, and $\phi \in C^2(\mathbb{R}^2)$ is D_4-symmetric satisfying $\phi(E(\cdot - \boldsymbol{c}_\phi) + \boldsymbol{c}_\phi) = \phi$ for all $E \in D_4$ with $\boldsymbol{c}_\phi := (1/2, -1/2)^T$.

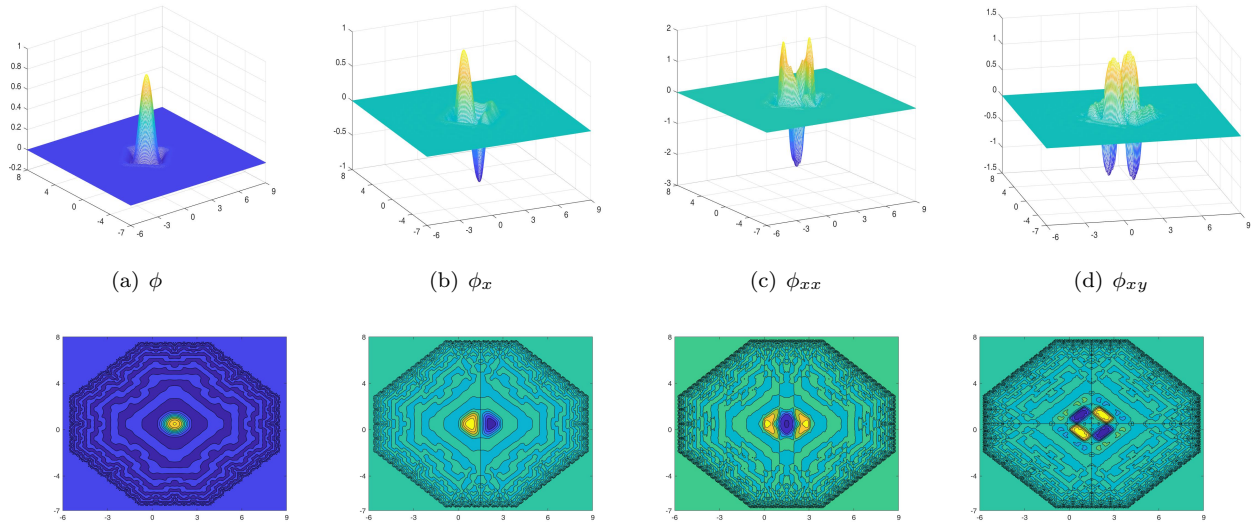

(a) ϕ (b) ϕ_x (c) ϕ_{xx} (d) ϕ_{xy}

(e) supp(ϕ) (f) supp(ϕ_x) (g) supp(ϕ_{xx}) (h) supp(ϕ_{xy})

Figure 4: (a)–(d) in the first row are respectively the refinable function ϕ (with the mask $\boldsymbol{a}^{2D}$ in (2.10) for $t = \frac{3}{512}$), its first order partial derivative $\frac{\partial \phi}{\partial x}$, and its second order partial derivatives $\frac{\partial^2 \phi}{\partial x^2}$ and $\frac{\partial^2 \phi}{\partial y \partial x}$. (e)–(h) in the second row are their corresponding contours. Note that $\mathrm{sr}(\boldsymbol{a}^{2D}, M_{\sqrt{2}}) = \mathrm{lpm}(\boldsymbol{a}^{2D}) = 6$, $\mathrm{sm}_2(\boldsymbol{a}^{2D}, M_{\sqrt{2}}) \approx 3.54575$ for mask $\boldsymbol{a}^{2D}$ with $t = \frac{3}{512}$, and $\phi \in C^2(\mathbb{R}^2)$ is D_4-symmetric satisfying $\phi(E(\cdot - \boldsymbol{c}_\phi) + \boldsymbol{c}_\phi) = \phi$ for all $E \in D_4$ with $\boldsymbol{c}_\phi := (1/2, -1/2)^T$.

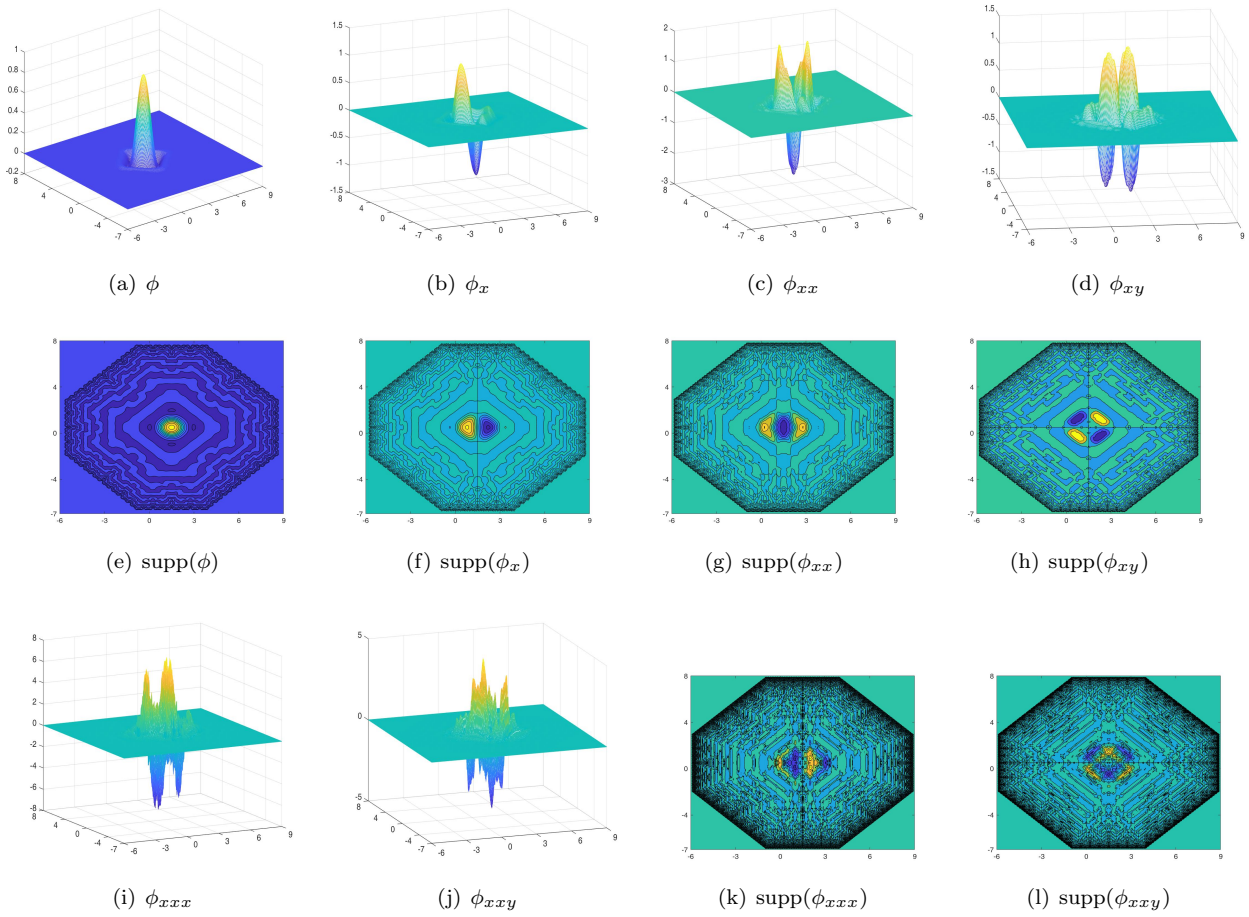

(a) ϕ (b) ϕ_x (c) ϕ_{xx} (d) ϕ_{xy}

(e) supp(ϕ) (f) supp(ϕ_x) (g) supp(ϕ_{xx}) (h) supp(ϕ_{xy})

(i) ϕ_{xxx} (j) ϕ_{xxy} (k) supp(ϕ_{xxx}) (l) supp(ϕ_{xxy})

Figure 5: (a)–(d) in the first row are respectively the refinable function ϕ (with the mask $\boldsymbol{a}^{2D}$ in (2.10) for $t = \frac{1}{128}$), its first order partial derivative $\frac{\partial \phi}{\partial x}$, and its second order partial derivatives $\frac{\partial^2 \phi}{\partial x^2}$ and $\frac{\partial^2 \phi}{\partial y \partial x}$. (e)–(h) in the second row are their corresponding contours. (i)–(l) in the third row are respectively its third order partial derivatives $\frac{\partial^3 \phi}{\partial x^3}$, $\frac{\partial^3 \phi}{\partial y \partial x^2}$ and their contours. Note that $\mathrm{sr}(\boldsymbol{a}^{2D}, M_{\sqrt{2}}) = \mathrm{lpm}(\boldsymbol{a}^{2D}) = 4$, $\mathrm{sm}_2(\boldsymbol{a}^{2D}, M_{\sqrt{2}}) \approx 3.73908$ for mask $\boldsymbol{a}^{2D}$ with $t = \frac{1}{128}$, and $\phi \in C^2(\mathbb{R}^2)$ is D_4-symmetric satisfying $\phi(E(\cdot - \boldsymbol{c}_\phi) + \boldsymbol{c}_\phi) = \phi$ for all $E \in D_4$ with $\boldsymbol{c}_\phi := (1/2, -1/2)^T$.

Remark 2.1. *It is known that, if the initial mesh consists of vertices specified by a sequence $\boldsymbol{v}$, and with constant valence 4 at all vertices, then the limiting surface of the subdivision scheme (2.1) is a linear combination of integer shifts of the refinable function ϕ with coefficients $\boldsymbol{v}$. By doing so, the limiting surface is C^2 smooth except at a finite number of isolated extraordinary vertices.*

3 Subdivision scheme

In this section, we give a demonstration of the implementation of the proposed subdivision scheme using the bivariate mask $\boldsymbol{a}^{2D}$ in (2.10) for the case $t = 0$, which is usually much easier to be implemented. Besides, we discuss the smoothness at extraordinary vertices. Notably, other cases when $t \neq 0$ can be analyzed similarly.

3.1 Split and connection rules

It is more convenient to use stencils for subdivision schemes in computer graphics than a filter/mask $\boldsymbol{a}$. Due to the fact that $|\det(M_{\sqrt{2}})| = 2$, the number of vertices of a mesh of quadrilaterals, to be called quads for short, is roughly doubled after each level subdivision of a $\sqrt{2}$-subdivision scheme.

The targets of $\sqrt{2}$-subdivision schemes are polyhedra or solid objects with the surface constructed in the quadrilateral mesh. For triangular meshes, other schemes such as the $\sqrt{3}$-subdivision schemes may be used. However, any surface in the triangular or mixed mesh can be easily converted into a surface in the quadrilateral-only mesh by using

the common trick: inserting the centroid or average of all the vertices of each polygonal face as a new vertex and connecting the centroid to the middle point of each side of the polygonal face. From this point of view, $\sqrt{2}$-subdivision schemes can also be applied to subdivide triangular surfaces. Moreover, such a trick is not necessary for our method since the new vertices are only inserted on each edge, details are presented in this section.

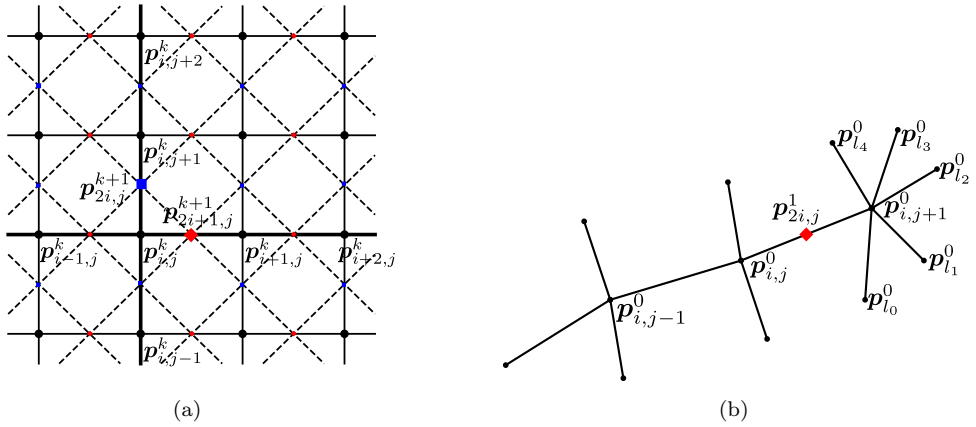

Figure 6: Illustration of the proposed dual $\sqrt{2}$-subdivision. (a) the black circles are vertices of the previous mesh $\boldsymbol{p}^k_{i,j}$, blue squares are subdivided vertices $\boldsymbol{p}^{k+1}_{2i,j}$ and red diamonds are $\boldsymbol{p}^{k+1}_{2i+1,j}$, illustrating the subdivision process in (3.1) with $\alpha = -\frac{1}{16}$ and $\beta = \frac{9}{16}$. (b) extraordinary vertices should be considered only for an initial mesh. Note that the valances of all vertices are 4 after applying the dual $\sqrt{2}$-subdivision once.

To facilitate our presentation, we first illustrate our subdivision scheme for regular quadrilateral meshes, that is, the valence of each vertex is 4. Notably, the subdivision stencils for the dual subdivision triplet $(\boldsymbol{a}; M_{\sqrt{2}}; D_4)$ are shown in Figure 1. The proposed $\sqrt{2}$-subdivision completes a subdivision step by inserting a new vertex of each edge into the mesh. Those new vertices are generated from the old ones. Let $\boldsymbol{p}^k_{i,j}$, $i = 0, \ldots, m$, $j = 0, \ldots, n$, be vertices of a level k mesh. Then a vertex $\boldsymbol{p}^{k+1}_{i,j}$ of the level $k+1$ mesh can be computed by

$$\begin{aligned} \boldsymbol{p}^{k+1}_{2i,j} &= \alpha \boldsymbol{p}^k_{i,j-1} + \beta \boldsymbol{p}^k_{i,j} + \beta \boldsymbol{p}^k_{i,j+1} + \alpha \boldsymbol{p}^k_{i,j+2}, \\ \boldsymbol{p}^{k+1}_{2i+1,j} &= \alpha \boldsymbol{p}^k_{i-1,j} + \beta \boldsymbol{p}^k_{i,j} + \beta \boldsymbol{p}^k_{i+1,j} + \alpha \boldsymbol{p}^k_{i+2,j}, \end{aligned} \tag{3.1}$$

where $\alpha, \beta \in \mathbb{R}$ and $2(\alpha + \beta) = 1$. In this paper, we focus on the case $\alpha = -\frac{1}{16}$ and $\beta = \frac{9}{16}$ as shown in Figure 1. The reason is that such a scheme will possess high polynomial preserving/interpolating property. It is natural that the mid-edge subdivision [25] is a special case of our method if we set $\alpha = 0$ and $\beta = \frac{1}{2}$. Note that the stencil in Figure 1 behaves essentially like a 1D stencil, which allows our proposed subdivision scheme to handle arbitrary polyhedra meshes easily. We shall discuss this issue in details later.

Notably, the new vertex $\boldsymbol{p}^{k+1}_{2i,j}$ is on the edge connecting vertices $\boldsymbol{p}^k_{i,j}$ and $\boldsymbol{p}^k_{i,j+1}$, and the new vertex $\boldsymbol{p}^{k+1}_{2i+1,j}$ is on the edge connecting vertices $\boldsymbol{p}^k_{i,j}$ and $\boldsymbol{p}^k_{i+1,j}$. New edges are inserted by connecting two new vertices "diagonally", thus we get new faces for each old face and each old vertex. Old vertices, edges, and faces are all removed from the new mesh, as shown in Figure 1. In other words, the scheme makes the mesh size grow at a factor of 2.

Such a subdivision scheme is a vertex split scheme, thus it can be performed on arbitrary polygonal meshes. However, for a general polyhedra mesh, there may be some vertices whose valence is not 4, which is usually called an extraordinary vertex. In this case, the above subdivision rules may cause some ambiguities. However, this would only happen for an initial mesh. Here we give a method to handle these vertices. Suppose the valence of a vertex $\boldsymbol{p}^0_{i,j+1}$ is 6, as shown in Figure 6(b), thus we may suppose $\boldsymbol{p}^0_{i,j+2} = \boldsymbol{p}^0_{i,j+1}$ when we try to compute $\boldsymbol{p}^1_{2i,j}$. Because the proposed method is a dual subdivision scheme, valences of all vertices become 4 for the new mesh after one round of subdivision, as shown in Figure 7. In other words, the particular rule is only necessary for the initial control mesh.

Notably, two steps of our subdivision scheme will lead to a mesh with the same topological connectivity as that of one step of the Doo-Sabin subdivision. In Figure 8 we show the stencils of two consecutive steps of the proposed subdivision scheme, as well as two consecutive steps of the mid-edge scheme and one step of Doo-Sabin scheme. Moreover, for the boundaries, we use a simple way to replicate boundary edges, *i.e.,* we create a quadrilateral with two coinciding pairs of vertices.

(a) (b)

Figure 7: A vertex of valence 6 of an initial mesh (a) becomes a hexagon (b) after one step of subdivision, and valences of all vertices are 4. A special subdivision rule for extraordinary vertices is required only for an initial mesh.

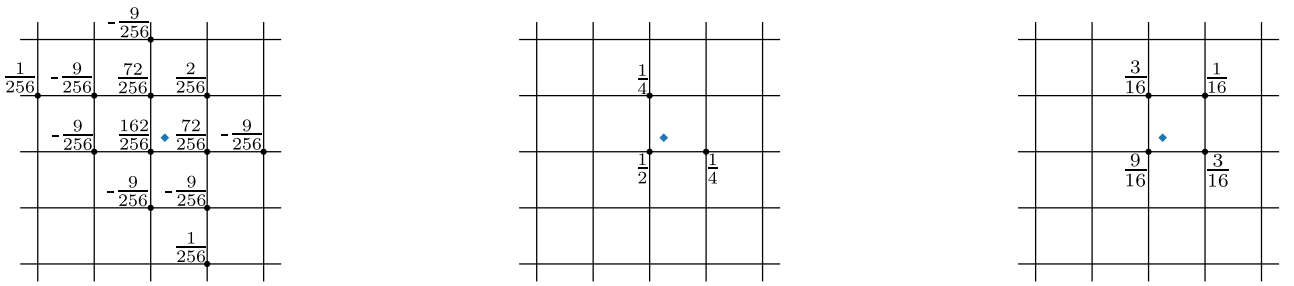

(a) Proposed $\sqrt{2}$-subdivision (b) Mid-edge subdivision (c) Doo-Sabin subdivision

Figure 8: Comparison of our $\sqrt{2}$-subdivision with mid-edge and Doo-Sabin subdivision. A new vertex is marked as a diamond, and old vertices for computing it are marked as circles. (a) The coefficients of old vertices for computing a new vertex after two proposed $\sqrt{2}$-subdivisions. (b) The coefficients of old vertices for computing a new vertex after two mid-edge subdivisions. (c) The coefficients of old vertices for computing a new vertex after one Doo-Sabin subdivision.

3.2 Subdivision matrix

An m neighborhood refers to m layers of vertices around a central n-gon, where the n-gon is counted as the first layer. Such an m neighborhood is said to be invariant if the level $k+1$ control points can be computed knowing only the level k control points in this neighborhood. It is known that there is a minimal invariant neighborhood for any subdivision scheme with finitely supported masks.

For the proposed $\sqrt{2}$ subdivision scheme, we can recognize that the smallest invariant neighbor is comprised of n blocks with each block containing 13 vertices. In order to perform smoothness analysis near extraordinary vertices [25, 26, 28], we have to consider an invariant stencil generated by adding a layer of vertices to the smallest invariant stencil, *i.e.,* there are 22 vertices. Fig 9(a) shows a sector of such a stencil in which a numbering fashion is given, Fig 9(b) gives a finer block with two adjacent coarser blocks for one step of the proposed subdivision process. On the other hand, the proposed subdivision scheme is a dual method, so we have to consider double steps of subdivision

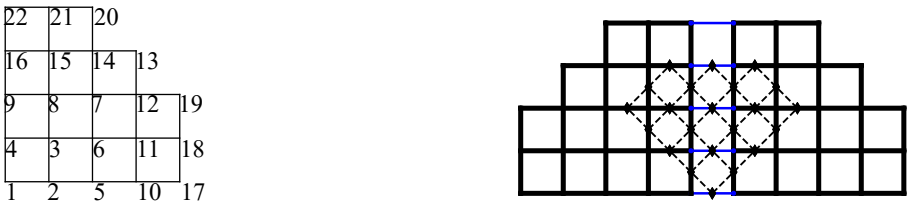

(a) (b)

Figure 9: Parts of an invariant stencil for smoothness analysis. (a) One block of the invariant stencil for continuity analysis and the label of vertices. (b) Two adjacent coarser blocks (bold) are connected by thin lines. One finer block is shown by dashed lines.

in order to in line with symmetric subdivision schemes [25].

For an invariant stencil, a subdivision matrix maps the vector of level k control points to the vector of level $k+1$ control points. Such a subdivision matrix plays an important role in the convergence and smoothness analysis of subdivision schemes [25, 26, 28]. In other words, the subdivision matrix A is a $22n \times 22n$ matrix at a vertex of valence n, which can be obtained by applying the subdivision operator (2.1) to the invariant stencil.

It is known that the eigenstructure of A can be investigated by considering the diagonal form of the matrix after a discrete Fourier transformation [25, 26]. Let

$$\hat{A}_k[:,1:5] = \begin{pmatrix}
2\alpha^2\boldsymbol{z}^{2k}+2(\alpha\beta+\beta^2)\boldsymbol{z}^k+2\beta^2 & 2\alpha\beta\boldsymbol{z}^k+\alpha\beta & 0 & 2\alpha\beta\boldsymbol{z}^k+\alpha\beta & \alpha^2\boldsymbol{z}^k \\
\alpha\beta\boldsymbol{z}^{2k}+(2\alpha\beta+\beta^2)\boldsymbol{z}^k+2\beta^2 & \alpha^2\boldsymbol{z}^{2k}+\alpha\beta\boldsymbol{z}^k+\alpha\beta+\beta^2 & \alpha\beta & 2\alpha^2\boldsymbol{z}^k+\alpha\beta & \alpha\beta \\
2\alpha\beta\boldsymbol{z}^k+2\beta^2 & \alpha\beta\boldsymbol{z}^k+\alpha\beta+\beta^2 & 2\alpha^2\boldsymbol{z}^k+2\alpha^2 & \alpha\beta\boldsymbol{z}^k+\alpha\beta+\beta^2 & \alpha\beta \\
\alpha\beta\boldsymbol{z}^{2k}+(2\alpha\beta+\beta^2)\boldsymbol{z}^k+2\beta^2 & 2\alpha^2\boldsymbol{z}^k+\alpha\beta & \alpha\beta & \alpha^2\boldsymbol{z}^{2k}+\alpha\beta\boldsymbol{z}^k+\alpha\beta+\beta^2 & 0 \\
2\alpha^2\boldsymbol{z}^k+\alpha\beta\boldsymbol{z}^k+\alpha\beta+\beta^2 & 2\beta^2 & \alpha\beta\boldsymbol{z}^k+\alpha\beta & (\alpha\beta+\beta^2)\boldsymbol{z}^k+\alpha\beta & \alpha\beta \\
2\alpha\beta\boldsymbol{z}^k+\alpha\beta+\beta^2 & \alpha^2\boldsymbol{z}^k+2\beta^2 & \alpha\beta+\beta^2 & \alpha\beta\boldsymbol{z}^k+2\alpha^2 & \alpha\beta \\
2\alpha^2 & \alpha\beta\boldsymbol{z}^k+\alpha\beta+\beta^2 & 2\beta^2 & \alpha\beta\boldsymbol{z}^k+\alpha\beta+\beta^2 & \alpha\beta \\
2\alpha\beta\boldsymbol{z}^k+\alpha\beta+\beta^2 & \alpha\beta\boldsymbol{z}^k+2\alpha^2 & \alpha\beta+\beta^2 & \alpha^2\boldsymbol{z}^k+2\beta^2 & 0 \\
(2\alpha^2+\alpha\beta)\boldsymbol{z}^k+\alpha\beta+\beta^2 & (\alpha\beta+\beta^2)\boldsymbol{z}^k+\alpha\beta & \alpha\beta\boldsymbol{z}^k+\alpha\beta & 2\beta^2 & \alpha^2+\alpha\beta\boldsymbol{z}^k \\
\alpha^2\boldsymbol{z}^{2k}+\alpha\beta\boldsymbol{z}^k+\alpha\beta & 2\beta^2 & \alpha\beta\boldsymbol{z}^k+\alpha\beta & (\alpha\beta+\beta^2)\boldsymbol{z}^k & \alpha\beta+\beta^2 \\
\alpha\beta & \alpha^2\boldsymbol{z}^k+2\beta^2 & \alpha\beta+\beta^2 & \alpha\beta\boldsymbol{z}^k+\alpha\beta & \alpha\beta+\beta^2 \\
\alpha^2\boldsymbol{z}^k+\alpha\beta & \alpha\beta+\beta^2 & 2\beta^2 & \alpha\beta\boldsymbol{z}^k+\alpha\beta & 2\alpha^2 \\
0 & \alpha\beta & 2\beta^2 & \alpha\beta & \alpha^2\boldsymbol{z}^k+\alpha\beta \\
\alpha^2\boldsymbol{z}^k+\alpha\beta & \alpha\beta\boldsymbol{z}^k+\alpha\beta & 2\beta^2 & \alpha\beta+\beta^2 & 0 \\
\alpha\beta & \alpha\beta\boldsymbol{z}^k+\alpha\beta & \alpha\beta+\beta^2 & \alpha^2\boldsymbol{z}^k+2\beta^2 & \alpha\beta\boldsymbol{z}^k \\
\alpha^2\boldsymbol{z}^{2k}+\alpha\beta\boldsymbol{z}^k+\alpha\beta & (\alpha\beta+\beta^2)\boldsymbol{z}^k & \alpha\beta\boldsymbol{z}^k+\alpha\beta & 2\beta^2 & 2\alpha^2\boldsymbol{z}^k \\
\alpha\beta & \alpha\beta+\beta^2 & \alpha\beta & 2\alpha^2\boldsymbol{z}^k & 2\beta^2 \\
\alpha\beta & \alpha\beta+\beta^2 & \alpha^2\boldsymbol{z}^k+2\alpha^2 & \alpha\beta\boldsymbol{z}^k & 2\beta^2 \\
0 & 2\alpha^2 & \alpha\beta+\beta^2 & \alpha\beta & \alpha\beta+\beta^2 \\
0 & \alpha\beta & \alpha\beta+\beta^2 & 2\alpha^2 & \alpha\beta\boldsymbol{z}^k \\
\alpha\beta & \alpha\beta\boldsymbol{z}^k & \alpha^2\boldsymbol{z}^k+2\alpha^2 & \alpha\beta+\beta^2 & \alpha\beta\boldsymbol{z}^k \\
\alpha\beta & 2\alpha^2\boldsymbol{z}^k & \alpha\beta & \alpha\beta+\beta^2 & (\alpha\beta+\beta^2)\boldsymbol{z}^k
\end{pmatrix},$$

$$\hat{A}_k[:,6:22] = \begin{pmatrix}
0 & 0 & 0 & \alpha^2\boldsymbol{z}^k & 0 & 0 & 0 & 0 & 0 & 0 & 0 & 0 & 0 & 0 & 0 & 0 & 0 \\
0 & 0 & \alpha^2 & 0 & 0 & 0 & 0 & 0 & 0 & 0 & 0 & 0 & 0 & 0 & 0 & 0 & 0 \\
0 & 0 & 0 & \alpha\beta & 0 & 0 & 0 & 0 & 0 & 0 & 0 & 0 & 0 & 0 & 0 & 0 & 0 \\
\alpha^2 & 0 & 0 & \alpha\beta & 0 & 0 & 0 & 0 & 0 & 0 & 0 & 0 & 0 & 0 & 0 & 0 & 0 \\
0 & 0 & 0 & \alpha^2+\alpha\beta\boldsymbol{z}^k & 0 & 0 & 0 & 0 & 0 & 0 & \alpha^2\boldsymbol{z}^k & 0 & 0 & 0 & 0 & 0 & 0 \\
\alpha\beta & 0 & \alpha\beta & 0 & 0 & \alpha^2 & 0 & 0 & 0 & 0 & 0 & 0 & 0 & 0 & 0 & 0 & 0 \\
\alpha\beta & 0 & \alpha\beta & \alpha\beta & \alpha^2 & 0 & 0 & 0 & 0 & 0 & \alpha^2 & 0 & 0 & 0 & 0 & 0 & 0 \\
\alpha\beta & 0 & \alpha\beta & \alpha\beta & 0 & 0 & 0 & 0 & 0 & \alpha^2 & 0 & 0 & 0 & 0 & 0 & 0 & 0 \\
0 & 0 & 0 & \alpha\beta & \alpha^2\boldsymbol{z}^k & 0 & 0 & 0 & 0 & 0 & 0 & 0 & 0 & 0 & 0 & 0 & 0 \\
\alpha\beta & \alpha^2 & 0 & 2\alpha^2\boldsymbol{z}^k & \alpha\beta & 0 & 0 & 0 & 0 & 0 & 0 & 0 & 0 & 0 & 0 & 0 & 0 \\
2\alpha^2 & 0 & \alpha^2\boldsymbol{z}^k+\alpha\beta & \alpha\beta\boldsymbol{z}^k & \alpha\beta & 0 & 0 & 0 & 0 & 0 & 0 & 0 & 0 & 0 & 0 & 0 & 0 \\
\alpha\beta+\beta^2 & \alpha\beta & \alpha\beta & 0 & 0 & \alpha\beta & 0 & 0 & \alpha^2 & 0 & 0 & 0 & 0 & 0 & 0 & 0 & 0 \\
\alpha\beta+\beta^2 & 2\alpha^2 & \alpha\beta+\beta^2 & \alpha^2\boldsymbol{z}^k+\alpha\beta & 0 & \alpha\beta & 0 & 0 & \alpha\beta & 0 & 0 & 0 & 0 & 0 & 0 & 0 & 0 \\
\alpha\beta & \alpha\beta & \alpha\beta+\beta^2 & 2\alpha^2 & 0 & 0 & \alpha^2 & 0 & 0 & \alpha\beta & 0 & 0 & 0 & 0 & 0 & 0 & 0 \\
\alpha^2\boldsymbol{z}^k+\alpha\beta & 0 & 2\alpha^2 & \alpha\beta+\beta^2 & 0 & 0 & 0 & 0 & 0 & 0 & \alpha\beta & 0 & 0 & 0 & 0 & 0 & 0 \\
0 & \alpha^2 & \alpha\beta & \alpha\beta+\beta^2 & 0 & 0 & 0 & 0 & 0 & 0 & \alpha\beta & 0 & 0 & 0 & 0 & 0 & 0 \\
\alpha\beta & 0 & \alpha^2+\alpha\beta\boldsymbol{z}^k & (\alpha\beta+\beta^2)\boldsymbol{z}^k & \alpha\beta & 0 & 0 & 0 & 0 & 0 & \alpha\beta\boldsymbol{z}^k & 0 & 0 & 0 & 0 & 0 & \alpha^2\boldsymbol{z}^k \\
\alpha\beta+\beta^2 & \alpha\beta & 0 & \alpha\beta\boldsymbol{z}^k & \alpha\beta & \alpha\beta & 0 & 0 & 0 & 0 & 0 & 0 & \alpha^2 & 0 & 0 & 0 & 0 \\
2\beta^2 & \alpha\beta & \alpha\beta & \alpha\beta\boldsymbol{z}^k & \alpha\beta & \alpha\beta & 0 & 0 & 0 & \alpha^2 & 0 & \alpha^2 & 0 & 0 & 0 & 0 & 0 \\
\alpha\beta & \alpha\beta & 2\beta^2 & \alpha\beta+\beta^2 & 0 & \alpha^2 & 0 & 0 & 0 & \alpha\beta & \alpha\beta & 0 & 0 & 0 & 0 & 0 & \alpha^2 \\
0 & \alpha\beta & \alpha\beta+\beta^2 & 2\beta^2 & 0 & 0 & 0 & 0 & 0 & \alpha\beta & \alpha\beta & 0 & 0 & 0 & 0 & \alpha^2 & 0 \\
\alpha^2+\alpha\beta\boldsymbol{z}^k & 0 & \alpha\beta & 2\beta^2 & \alpha\beta\boldsymbol{z}^k & 0 & 0 & 0 & 0 & 0 & \alpha\beta & \alpha^2\boldsymbol{z}^k & 0 & 0 & 0 & 0 & 0
\end{pmatrix},$$

where $k = 0, 1, \ldots, n-1$, $\boldsymbol{z} = e^{\mathbf{i}\frac{2\pi}{n}}$. Then, A is similar to $\mathrm{diag}\{\hat{A}_0, \hat{A}_1, \ldots, \hat{A}_{n-1}\}$. Hence all eigenvalues of A can be obtained by calculating the eigenvalues of $\hat{A}_k$.

3.3 Smoothness analysis at extraordinary vertices

Following the proposed subdivision rules, a vertex of valence n will produce an n-gon on the limit surface, which is usually called an extraordinary vertex if $n \neq 4$. According to the theory of continuity analysis near extraordinary vertices [26], C^1 continuity proof can be achieved by showing that the four leading eigenvalues of A meet the condition below, *i.e.,*

$$\lambda_0 = 1 > \lambda_1 = \lambda_2 > |\lambda_3|,$$

and that the characteristic map defined by the pair of eigenvectors of the two subdominant eigenvalues λ_1 and λ_2 is regular and injective.

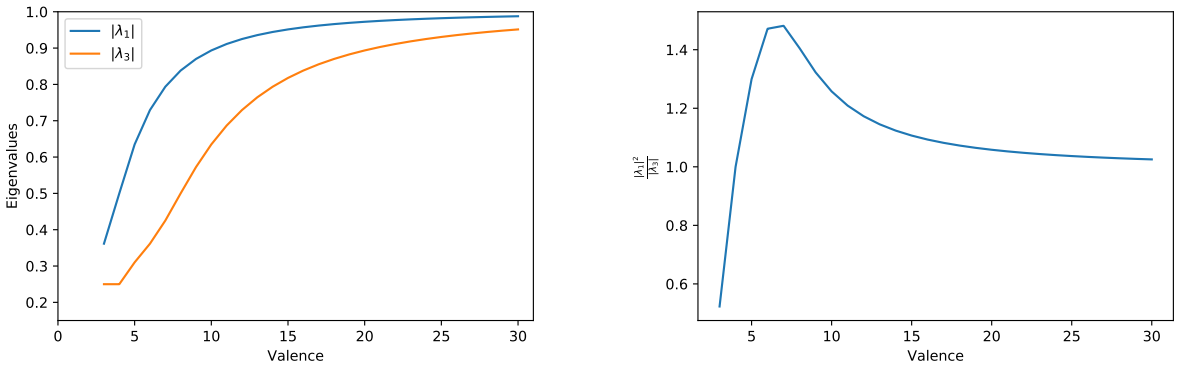

(a) (b)

Figure 10: (a) is the magnitude curves of subdominant and subsubdominant eigenvalues $|\lambda_1|$ and $|\lambda_3|$, (b) is the magnitude curve of $\frac{|\lambda_1|^2}{|\lambda_3|}$ in terms of valence n from 3 to 30.

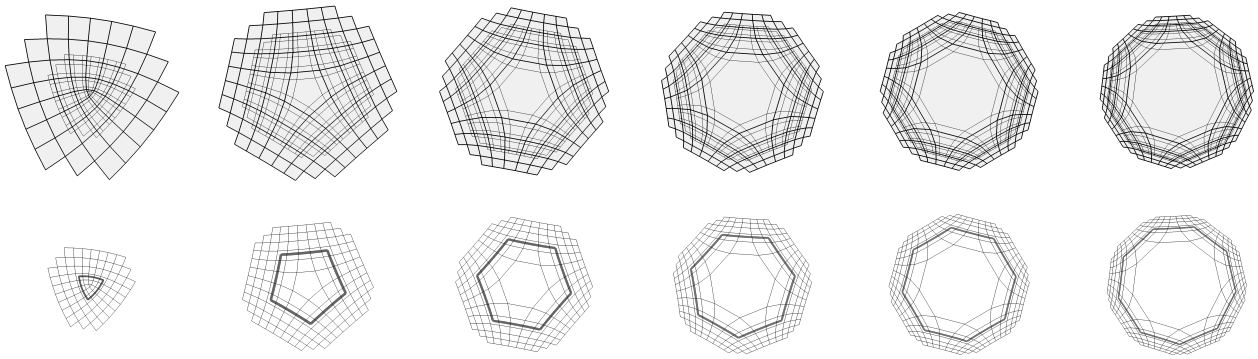

(a) $n = 3$ (b) $n = 5$ (c) $n = 6$ (d) $n = 7$ (e) $n = 8$ (f) $n = 9$

Figure 11: Top row gives control meshes of characteristic maps for the proposed subdivision scheme at extraordinary vertices with valences $n = 3, 5, 6, 7, 8, 9$, the control mesh after two subdivision steps are shown with thin lines. Bottom row gives the control mesh for rings of the characteristic maps (the limit patches are shown in gray).

In most cases, it is difficult to perform theoretical analysis for the regularity and injectivity for all subdivision schemes [25, 26]. Thus, numerical evidence has to be provided to verify the regularity and injectivity of the characteristic map.

For numerical analysis, the surface generated by subdividing an initial mesh topologically identical to the invariant neighborhood is defined as the characteristic map. If the subdominant eigenvalues $\lambda_1 = \lambda_2$ of A are real, then coordinates of control points come from the two corresponding eigenvectors, respectively. The regularity of the map can be examined by its behavior on a ring around an extraordinary vertex [26, 28, 24].

In our implementation, we give numerical results for the smooth analysis at extraordinary vertices. Because the proposed subdivision scheme is a $\sqrt{2}$-subdivision, we perform the spectrum analysis for double steps [25]. Thus we have two real subdominant eigenvalues. Figure 10 demonstrates the curves of $|\lambda_1|$, $|\lambda_3|$, and $\frac{|\lambda_1|^2}{|\lambda_3|}$ in terms of valence n ranging from 3 to 30. Figure 11 gives some examples for the control mesh of characteristic maps at extraordinary vertices with valences $n = 3, 5, 6, 7, 8, 9$. We further compute the Fourier indices of the subdominant eigenvalues which are located at 1 and $n - 1$ [24]. It is sufficient that the proposed subdivision scheme satisfies the C^1 continuity near extraordinary vertices.

4 Experimental results

In this section, we provide several numerical examples to demonstrate the performance of our method. We show that resultant surfaces have almost the same shape produced by the dual $\sqrt{2}$-subdivision using masks $\boldsymbol{a}^{2D}$ in (2.10) with

three different choices of the parameter $t \in \{0, \frac{3}{512}, \frac{1}{128}\}$. This is not surprising because Figures 3, 4 and 5 show that all their associated basis/refinable functions look very similar to each other.

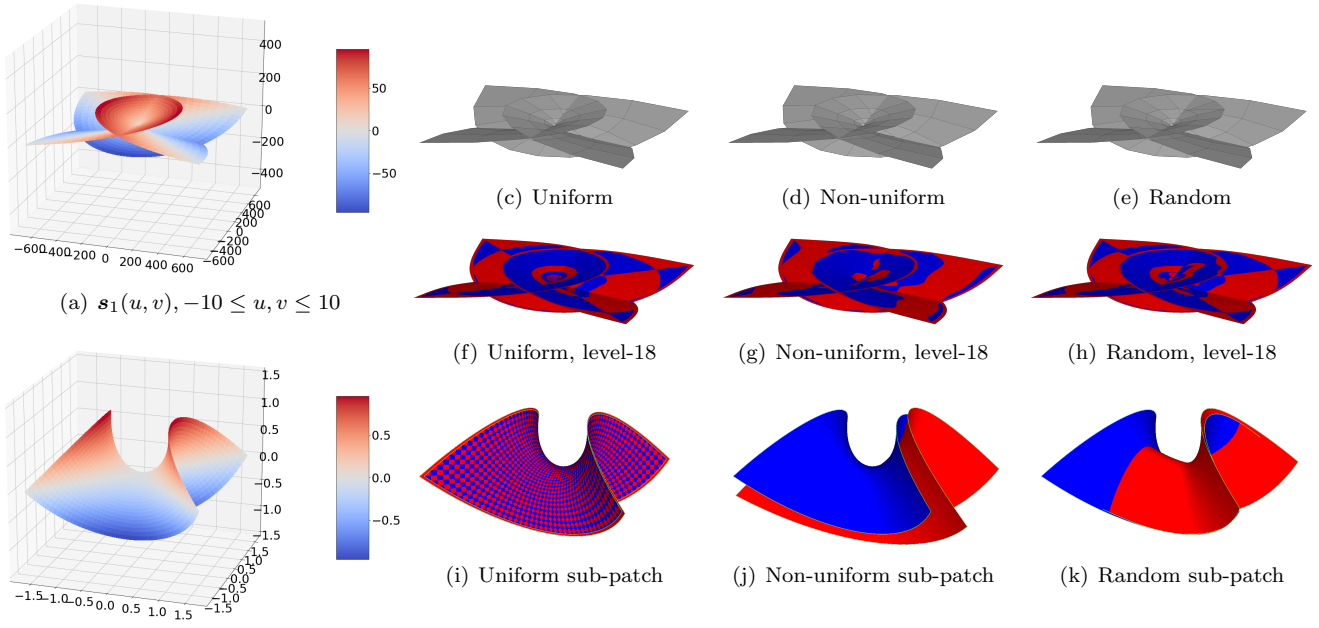

(a) $\boldsymbol{s}_1(u,v), -10 \le u,v \le 10$ (b) $\boldsymbol{s}_1(u,v), -1 \le u,v \le 1$ (c) Uniform (d) Non-uniform (e) Random (f) Uniform, level-18 (g) Non-uniform, level-18 (h) Random, level-18 (i) Uniform sub-patch (j) Non-uniform sub-patch (k) Random sub-patch

Figure 12: A parametric surface (a) and a smaller one (b) are given by $\boldsymbol{s}_1(u,v) = (\frac{1}{3}u^3 - u - uv^2, -u^2v - v + \frac{1}{3}v^3, u^2 - v^2)$ with the parameter domains $(u,v) \in [-10,10]^2$ and $(u,v) \in [-1,1]^2$, respectively. (c)-(e) are the input initial meshes with 11×11 vertices by uniformly, non-uniformly, and randomly sampling (a) within $(u,v) \in [-10,10]^2$. (f)- (h) are the level-18 subdivided surfaces in red (using $t = 0$) together with the original parametric surface $\boldsymbol{s}_1(u,v), (u,v) \in [-10,10]^2$ in blue. Removing boundary affected vertices, (i)-(k) show sub-patches of the smaller subdivided surfaces in red together with their corresponding smaller parametric surface $\boldsymbol{s}_1(u,v), (u,v) \in [-1,1]^2$ in blue. (i) shows that our quasi-interpolating dual subdivision scheme agrees well with the cubic polynomial parametric surface if the initial control mesh is obtained through uniformly sampling and if the vertices affected by boundaries are removed.

Before applying our quasi-interpolating dual $\sqrt{2}$-subdivision schemes to some general polyhedra initial meshes, we perform two experiments to demonstrate the quasi-interpolation property of our proposed subdivision schemes. In the first experiment, we generate three types of initial meshes by sampling a cubic polynomial parametric surface uniformly, non-uniformly or randomly; then we apply our quasi-interpolating dual $\sqrt{2}$-subdivision scheme with the particular choice $t = 0$ to all such initial meshes. Figure 12 shows that the generated subdivision surface agrees well with the given parametric surface if the input initial mesh is obtained through the uniform sampling of a cubic polynomial parametric surface, while non-uniform and random samplings yield visible deviations. In the second experiment, we generate an initial mesh by uniformly sampling a parametric surface of polynomials of degree 5; then we apply our quasi-interpolating dual $\sqrt{2}$-subdivision schemes with the three choices $t = 0, \frac{3}{512}$ and $\frac{1}{128}$. Figure 13 shows that the generated subdivision surface with the choice $t = \frac{3}{512}$ agrees well with the given parametric surface (because the subdivision scheme with $t = \frac{3}{512}$ can interpolate all polynomials of degree up to 5), while the subdivision surfaces with the choices $t = 0, \frac{1}{128}$ yield large deviations (because they only interpolates polynomials of degree up to 3).

- Example 1. We consider in Figure 12 a cubic polynomial parametric surface below:

$$\boldsymbol{s}_1(u,v) = (T_1(u,v), T_2(u,v), T_3(u,v)) = \left(\frac{u^3}{3} - u - uv^2, -u^2v - v + \frac{v^3}{3}, u^2 - v^2\right).$$

Figure 12 plots the parametric surface $\boldsymbol{s}_1(u,v)$ with the parameter domain $(u,v) \in [-10,10]^2$. The three different input meshes in Figures 12(c)-12(e) are obtained by uniformly, non-uniformly, and randomly sampling this parametric surface within the parameter domain $(u,v) \in [-10,10]^2$. In particular, the non-uniform sampled parameter values for the vertices of Figure 12(d) are

$$u[0:10] = \{-10, -8.1, -5.9, -4.2, -2.1, 0, 1.9, 4.1, 6.2, 8.1, 10\},$$
$$v[0:10] = \{-10, -7.9, -6.1, -3.9, -2.1, 0, 2.1, 3.9, 5.9, 7.9, 10\}.$$

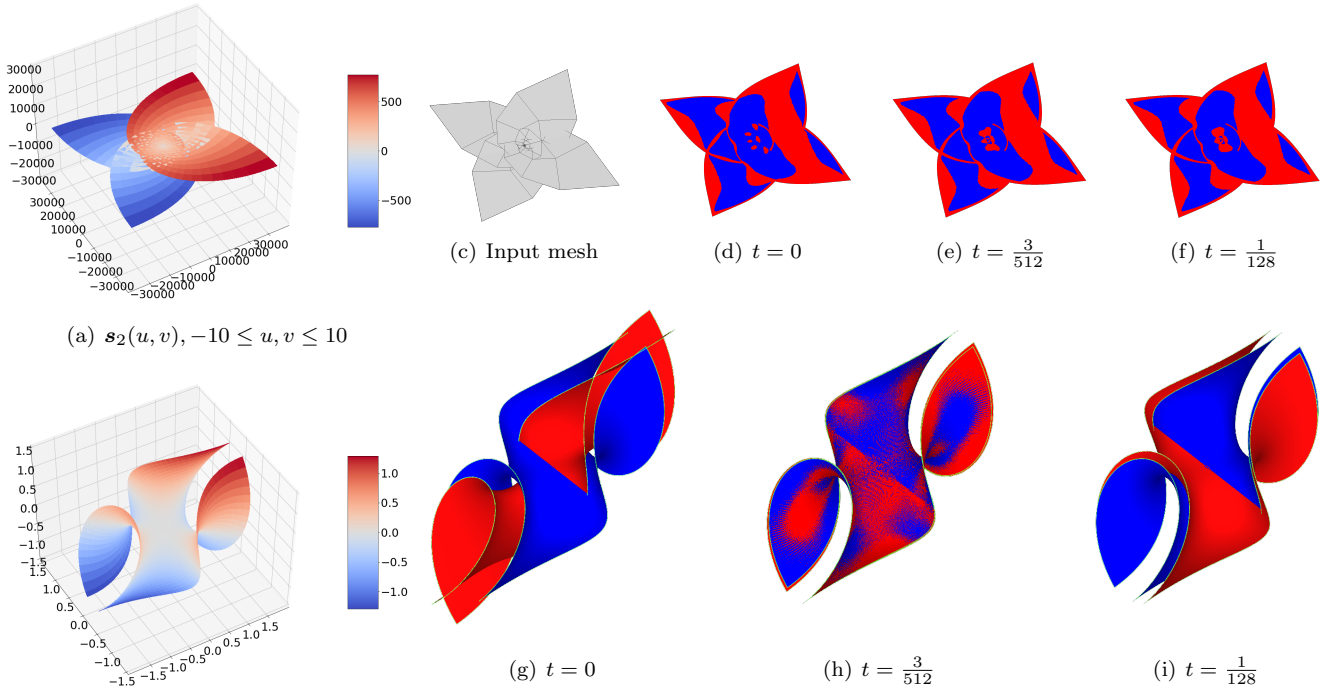

(a) $\boldsymbol{s}_2(u,v), -10 \le u,v \le 10$ (c) Input mesh (d) $t=0$ (e) $t=\frac{3}{512}$ (f) $t=\frac{1}{128}$

(b) $\boldsymbol{s}_2(u,v), -1 \le u,v \le 1$ (g) $t=0$ (h) $t=\frac{3}{512}$ (i) $t=\frac{1}{128}$

Figure 13: A parametric surface (a) and a smaller one (b) are given by $\boldsymbol{s}_2(u,v) = (\frac{1}{5}u^5 - 2u^3v^2 + uv^4 - u, u^4v - 2u^2v^3 + v + \frac{1}{5}v^5, \frac{2}{3}u^3 - 2uv^2)$ with the parameter domains $(u,v) \in [-10,10]^2$ and $(u,v) \in [-1,1]^2$, respectively. (c) is the input initial mesh with 11×11 vertices by uniformly sampling the parametric surface in (a). (d)-(f) give the level-18 subdivided results for the three choices $t = 0, \frac{3}{512}, \frac{1}{128}$, respectively, where we plot the subdivided surfaces in red together with the parametric surface in blue. Removing boundary affected vertices, (g)-(i) show the comparison of the sub-patches (i.e., portions of the smaller subdivision surfaces in (d)-(f)) with their corresponding portions in (a). Figure 13(h) shows that the generated subdivision surface with the choice $t = \frac{3}{512}$ agrees well with the parametric surface, while the subdivision surfaces in 13(g) and 13(i) with the choices $t = 0, \frac{1}{128}$ yield large deviations, because any choice $t \neq \frac{3}{512}$ only interpolates polynomials of degree up to 3.

To preserve the boundary for the given input meshes, we add 5 layers of their boundary vertices and perform 18 steps of the proposed subdivision with the choice $t = 0$. Figures 12(f)-12(h) show the subdivision results, where the subdivided surface is plotted in the red color together with the parametric surface in the blue color. Because we plot two surfaces together using different colors (red and blue) for the purpose of comparison, it may not be obviously easy to visualize both two surfaces well and to tell apart their differences. Nevertheless, from these figures in Figures 12(f)-12(h) we may observe some deviations close to boundaries due to lack of information beyond the boundaries.

To better demonstrate the quasi-interpolating property of the proposed subdivision scheme, we obtain small sub-patches of the subdivided surfaces by removing all vertices affected by boundary vertices through the subdivision process. Figures 12(i)-12(k) draw the resulting sub-patch of smaller subdivision surface in red together with its corresponding smaller parametric surface $\boldsymbol{s}_1(u,v)$ in blue within the smaller parameter domain $(u,v) \in [-1,1]^2$. We see clearly from Figure 12(i) that our proposed quasi-interpolating dual subdivision scheme with the choice $t = 0$ recovers well the parametric surface if the initial control mesh is obtained by uniformly sampling a cubic polynomial parametric surface and if the vertices affected by boundaries are removed.

- Example 2. Now we consider the second experiment in order to explain the differences of our proposed subdivision schemes using the 2D mask (2.10) with three different choices $t = 0, \frac{3}{512}$ and $\frac{1}{128}$. According to our previous discussion, the scheme can reproduce polynomials of degree up to 5 only with the choice $t = \frac{3}{512}$. We consider a quintic polynomial parametric surface below:

$$\boldsymbol{s}_2(u,v) = \left(\frac{1}{5}u^5 - 2u^3v^2 + uv^4 - u, u^4v - 2u^2v^3 + v + \frac{1}{5}v^5, \frac{2}{3}u^3 - 2uv^2\right).$$

Figure 13(a) and its sub-patch in Figure 13(b) plot the quintic polynomial parametric surfaces within the pa-

rameter domains $[-10,10]^2$ and $[-1,1]^2$, respectively. The 11×11 vertices of the input mesh are uniformly sampled from the parametric surface within $[-10,10]^2$, as shown in Figure 13(c). The proposed subdivision schemes are performed on the input mesh with three different choices $t = 0, \frac{3}{512}$ and $\frac{1}{128}$. Figures 13(d)-13(f) give the level-18 subdivided surfaces, where the subdivided surfaces are shown in red together with the parametric surface $\boldsymbol{s}_2(u,v)$, $(u,v) \in [-10,10]^2$ in blue. Although the different choices of t yield visually the same surfaces in Figures 13(d)-13(f), they are indeed different in Figures 13(g)-13(i) if we remove vertices affected by boundaries through the subdivision process. In particular, Figure 13(h) shows that the subdivision surface with the choice $t = \frac{3}{512}$ agrees well with the quintic polynomial parametric surface because this choice $t = \frac{3}{512}$ can interpolate all polynomials of degree up to 5, while the subdivision surfaces in Figures 13(g) and 13(i) with the choices $t = 0, \frac{1}{128}$ yield large deviations, because they only interpolate polynomials of degree up to 3.

- Example 3. Figure 14(a) gives an example of a 4-cube seat-shape polyhedron with 20 vertices and 18 quads. We perform the proposed subdivision scheme for 10 steps with different choices $t = 0, \frac{3}{512}, \frac{1}{128}$. Figures 14(b)-14(d) show that the resultant subdivided surfaces are visually almost the same, where each subdivided surface contains 18432 vertices and 36860 quads.

- Example 4. Figure 15(a) gives a chess king with 314 vertices and 312 quads. After 10 steps of the proposed dual $\sqrt{2}$-subdivision, we get three meshes (see Figures 15(b)-15(d)) with 319488 vertices and 638972 quads with different choices $t = 0, \frac{3}{512}$, and $\frac{1}{128}$, respectively. We can see that the subdivided surfaces have almost the same shape.

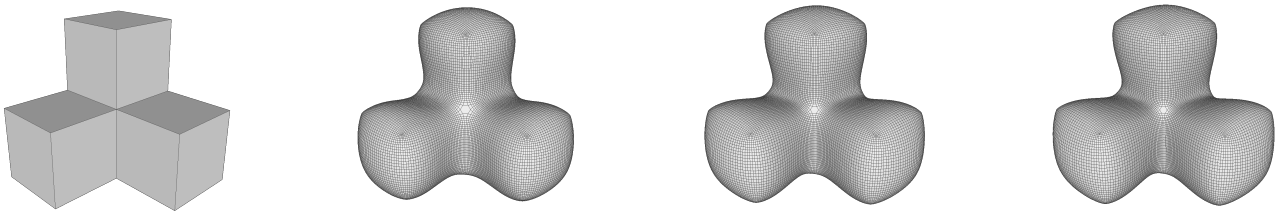

(a) Input mesh (b) $t = 0$ (c) $t = \frac{3}{512}$ (d) $t = \frac{1}{128}$

Figure 14: Results of applying the proposed $\sqrt{2}$-subdivision scheme to 4-cube seat-shape polyhedron with $t = 0, \frac{3}{512}, \frac{1}{128}$, respectively.

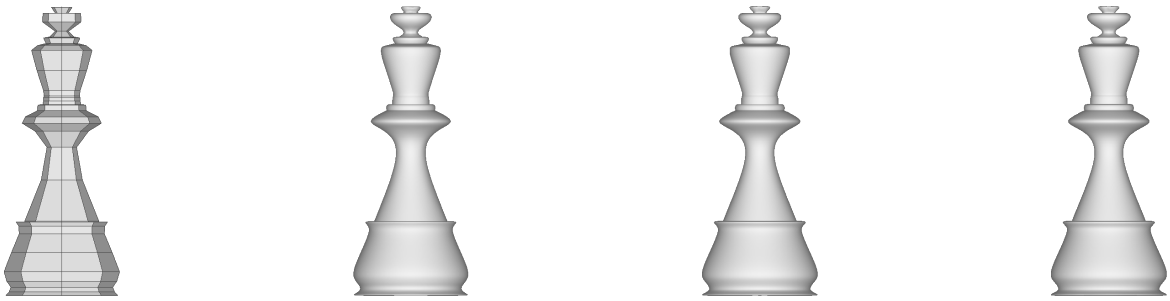

(a) Input mesh (b) $t = 0$ (c) $t = \frac{3}{512}$ (d) $t = \frac{1}{128}$

Figure 15: Results of applying the proposed $\sqrt{2}$-subdivision scheme to a chess king mesh with $t = 0, \frac{3}{512}, \frac{1}{128}$, respectively.

5 Conclusion

Inspired by the linear-phase moments and polynomial reproduction of 1D masks, we introduce a novel dual $\sqrt{2}$-subdivision scheme using essentially the 1D 4-point stencil in this paper. There are several advantages for such a subdivision scheme. First, it is quite easy to be implemented since 1D stencils are used to perform the subdivision. Besides, no additional rules are required for extraordinary and boundary vertices. Second, theoretical analysis shows

the proposed scheme can reproduce bivariate polynomials of high orders, and we further verify the results by performing several numerical examples. We believe the quasi-interpolating property could be interesting in the setting of CAGD. Finally, we claim that the smoothness at ordinary vertices and extraordinary vertices are C^2 and C^1, respectively.

Acknowledgment: The authors thank the anonymous referees for their helpful suggestions and comments. Research of Lincong Fang was supported by the Zhejiang Provincial Natural Science Foundation of China under Grant No. LY18F020023. Research of Bin Han was supported in part by the Natural Sciences and Engineering Research Council of Canada (NSERC) under Grant RGPIN-2019-04276. Research of Yi Shen was supported by the Zhejiang Provincial Natural Science Foundation of China under Grant No. LR19A010001 and the Natural Science Foundation of China under Grant No. 12022112.

References

[1] Catmull E., Clark J.. Recursively generated B-spline surfaces on arbitrary topological meshes. Computer-Aided Design, 1978, 10(6), 350–355.

[2] Chui, C. K., Jiang, Q., Ndao, R. N., 2007. Triangular and quadrilateral subdivision schemes: Regular case. Journal of Mathematical Analysis & Applications, 338(2), 1204–1223.

[3] Deslauriers, G., Dubuc, S., 1989. Symmetric iterative interpolation processes. Constructive Approximation, 5(1), 49–68.

[4] Doo, D., Sabin, M., 1978. Behaviour of recursive division surfaces near extraordinary points. Computer-Aided Design, 10(6), 356–360.

[5] Dyn, N., Hormann, K., Sabin, M., Shen, Z. 2008. Polynomial reproduction by symmetric subdivision schemes. Journal of Approximation Theory, 155(1), 28–42.

[6] Han, B., 2003. Classification and construction of bivariate subdivision schemes. Curve and surface fitting (Saint-Malo, 2002), Mod. Methods Math. Nashboro Press, Brentwood, TN, 187–197.

[7] Han, B., 2003. Computing the smoothness exponent of a symmetric multivariate refinable function. SIAM Journal on Matrix Analysis and Applications, 24(3), 693–714.

[8] Han, B., 2017. Framelets and wavelets. Applied and Numerical Harmonic Analysis, Birkhäuser/Springer, Cham, Algorithms, analysis, and applications, xxxiii + 724.

[9] Han, B., 2013. Properties of discrete framelet transforms. Mathematical Modelling of Natural Phenomena, 8(1), 18–47.

[10] Han, B., 2010. Symmetric orthonormal complex wavelets with masks of arbitrarily high linear-phase moments and sum rules. Advances in Computational Mathematics, 32(2), 209–237.

[11] Han, B., 2011. Symmetric orthogonal filters and wavelets with linear-phase moments. Journal of Computational and Applied Mathematics, 236(4), 482–503.

[12] Han, B., 2002. Symmetry property and construction of wavelets with a general dilation matrix. Linear Algebra and its Applications, 353(1), 207–225.

[13] Han, B., 2003. Vector cascade algorithms and refinable function vectors in Sobolev spaces. Journal of Approximation Theory, 124(1), 44–88.

[14] Han, B., Jia R. Q., 2002. Quincunx fundamental refinable functions and quincunx biorthogonal wavelets. Mathematics of Computation, 71(237), 165–196.

[15] Han, B., Jiang, Q., Shen, Z., Zhuang, X., 2018. Symmetric canonical quincunx tight framelets with high vanishing moments and smoothness. Mathematics of Computation, 87(309), 347–379.

[16] Ivrissimtzis, I. P., Dodgson, N. A., Sabin, M., 2005. $\sqrt{5}$-subdivision. Advances in Multiresolution for Geometric Modelling, 285–299.

[17] Jiang, Q., 2001. Matlab routines for Sobolev and Hölder smoothness computations of refinable functions. Available: http:\\ www.cs.umsl.edu\jiang\Jsoftware.htm.

[18] Lian, J. A., Yang, Y., 2010. A new cross subdivision scheme for surface design. Journal of Mathematical Analysis & Applications, 374(1), 244–257.

[19] Jiang, Q., Oswald, P., 2003. Triangular $\sqrt{3}$-subdivision schemes: the regular case. Journal of Computational and Applied Mathematics, 156(1), 47–75.

[20] Li, G., Ma, W., 2007. Composite $\sqrt{2}$ subdivision surfaces. Computer Aided Geometric Design, 24(6), 339–360.

[21] Li, G., Ma, W., Bao, H., 2004. $\sqrt{2}$ Subdivision for quadrilateral meshes. The Visual Computer, 20(2-3), 180–198.

[22] Mortenson, M.E., Geometric Modeling. Wiley: New York, NY, USA, 1985; pp. 305–317.

[23] Oswald P., Schröder P. Composite primal/dual $\sqrt{3}$-subdivision schemes. Computer Aided Geometric Design, 2003, 20(3): 135–164.

[24] Peters, J., Reif, U., 2008. Subdivision surfaces. Springer Berlin Heidelberg.

[25] Peters, J., Reif, U., 1997. The simplest subdivision scheme for smoothing polyhedra. ACM Transactions on Graphics, 16(4), 420–431.

[26] Reif, U., 1995. A unified approach to subdivision algorithms near extraordinary vertices. Computer Aided Geometric Design, 12(2), 153–174.

[27] Velho, L., Zorin, D., 2001. 4-8 subdivision. Computer Aided Goemtric Design, 18(5), 397–427.

[28] Zorin, D., Schröder, P., 2001. A unified framework for primal/dual quadrilateral subdivision schemes. Computer Aided Geometric Design, 18(5), 429–454.

Appendix: Proof of Theorem 2.1

Proof of Theorem 2.1. By the definition of the 2D mask $\boldsymbol{a}^{2D}$ in (1.3), we observe that for $j_1, j_2 \in \mathbb{N}_0$,

$$\begin{aligned}\sum_{k_1+k_2 \text{ is even}, k_1,k_2\in\mathbb{Z}} \boldsymbol{a}^{2D}(k_1,k_2)k_1^{j_1}k_2^{j_2} &= \frac{1}{2}\sum_{k\in\mathbb{Z}} \boldsymbol{a}^{1D}(k)k^{j_1+j_2},\\ \sum_{k_1+k_2 \text{ is odd}, k_1,k_2\in\mathbb{Z}} \boldsymbol{a}^{2D}(k_1,k_2)k_1^{j_1}k_2^{j_2} &= \frac{1}{2}\sum_{k\in\mathbb{Z}} \boldsymbol{a}^{1D}(k)k^{j_1}(1-k)^{j_2}.\end{aligned} \tag{5.1}$$

By (5.1) and (2.5), the 2D mask $\boldsymbol{a}^{2D}$ has order m sum rules with respect to the dilation matrix $M_{\sqrt{2}}$ if and only if

$$\sum_{k\in\mathbb{Z}} \boldsymbol{a}^{1D}(k)k^{j_1+j_2} = \sum_{k\in\mathbb{Z}} \boldsymbol{a}^{1D}(k)k^{j_1}(1-k)^{j_2}, \qquad \forall\, j_1, j_2 \in \mathbb{N}_0,\ j_1+j_2 < m. \tag{5.2}$$

- (1)⇒(2). Suppose that the mask $\boldsymbol{a}^{2D}$ has order m sum rules with respect to the dilation matrix $M_{\sqrt{2}}$. Then (5.2) holds true. For $1 \le j < m$, the above identities in (5.2) with $j_1 = j-1$ and $j_2 = 1$ imply

  $$S_j := \sum_{k\in\mathbb{Z}} \boldsymbol{a}^{1D}(k)k^j = \sum_{k\in\mathbb{Z}} \boldsymbol{a}^{1D}(k)k^{j-1}(1-k) = S_{j-1} - S_j,$$

  from which we must have $S_j = 2^{-1}S_{j-1}$ for all $j = 1, \ldots, m-1$. By our assumption, we have

  $$S_0 = \sum_{k\in\mathbb{Z}} \boldsymbol{a}^{1D}(k) = 1.$$

  Consequently, we must have $S_j = 2^{-j}$ for all $j = 0, \ldots, m-1$. This proves (1)⇒(2).

- (2)⇒(1). By item (2), we have $S_j := \sum_{k\in\mathbb{Z}} \boldsymbol{a}^{1D}(k)k^j = 2^{-j}$ for all $j = 0, \ldots, m-1$. Then

  $$\begin{aligned}\sum_{k\in\mathbb{Z}} \boldsymbol{a}^{1D}(k)k^{j_1}(1-k)^{j_2} &= \sum_{\ell=0}^{j_2}\sum_{k\in\mathbb{Z}} \frac{j_2!}{\ell!(j_2-\ell)!}(-1)^\ell k^\ell \boldsymbol{a}^{1D}(k)k^{j_1+\ell} = \sum_{\ell=0}^{j_2} \frac{j_2!}{\ell!(j_2-\ell)!}(-1)^\ell S_{j_1+\ell}\\ &= \sum_{\ell=0}^{j_2} \frac{j_2!}{\ell!(j_2-\ell)!}(-1)^\ell 2^{-j_1-\ell} = 2^{-j_1}\sum_{\ell=0}^{j_2} \frac{j_2!}{\ell!(j_2-\ell)!}(-2^{-1})^\ell\\ &= 2^{-j_1}(1-2^{-1})^{j_1} = 2^{-j_1-j_2} = S_{j_1+j_2} = \sum_{k\in\mathbb{Z}} \boldsymbol{a}^{1D}(k)k^{j_1+j_2}\end{aligned}$$

for all $j_1, j_2 \in \mathbb{N}$ with $j_1 + j_2 < m$. This proves (5.2). Consequently, the 2D mask $\boldsymbol{a}^{2D}$ must have order m sum rules with respect to the dilation matrix $M_{\sqrt{2}}$. This proves (2)⇒(1).

Obviously, the mask $\boldsymbol{a}^I$ defined in (2.8) is interpolating because $\boldsymbol{a}^I(2k) = 0$ for all $k \in \mathbb{Z}\backslash\{0\}$. Moreover, by (2.8), we have

$$\sum_{k\in\mathbb{Z}} \boldsymbol{a}^I(1+2k)(1+2k)^j = \frac{1}{2}\sum_{k\in\mathbb{Z}} \boldsymbol{a}^{1D}(-k)(1+2k)^j = \frac{1}{2}\sum_{k\in\mathbb{Z}} \boldsymbol{a}^{1D}(k)(1-2k)^j \quad \text{and} \quad \sum_{k\in\mathbb{Z}} \boldsymbol{a}^I(2k)(2k)^j = \frac{1}{2}\delta(j),$$

where $\delta(0) := 1$ and $\delta(k) = 0$ for all $k \in \mathbb{Z}\backslash\{0\}$. Note that

$$\sum_{k\in\mathbb{Z}} \boldsymbol{a}^{1D}(k)(1-2k)^j = \sum_{\ell=0}^{j}\sum_{k\in\mathbb{Z}} \frac{j!}{\ell!(j-\ell)!}\boldsymbol{a}^{1D}(k)(-2k)^\ell = \sum_{\ell=0}^{j}\frac{j!}{\ell!(j-\ell)!}(-2)^\ell S_\ell.$$

Consequently, by (2.4), the interpolating mask $\boldsymbol{a}^I$ has order m sum rules with respect to the dilation factor 2 if and only if

$$\sum_{\ell=0}^{j}\frac{j!}{\ell!(j-\ell)!}(-2)^\ell S_\ell = \delta(j), \qquad \text{for all } j = 0, \dots, m-1. \tag{5.3}$$

- (2)⇒(3). If item (2) holds true, then $S_j = 2^{-j}$ for all $j = 0, \dots, m-1$ and we deduce that for $j = 1, \dots, m-1$,

$$\sum_{\ell=0}^{j}\frac{j!}{\ell!(j-\ell)!}(-2)^\ell S_\ell = \frac{1}{2}\sum_{\ell=0}^{j}\frac{j!}{\ell!(j-\ell)!}(-1)^\ell = \frac{1}{2}(1-1)^j = 0$$

  and for $j = 0$, we obviously have $\sum_{\ell=0}^{j}\frac{j!}{\ell!(j-\ell)!}(-2)^\ell S_\ell = S_0 = 1$. Therefore, the interpolating mask $\boldsymbol{a}^I$ has order m sum rules with respect to the dilation factor 2. This proves (2)⇒(3).

- (3)⇒(2). Since item (3) holds true, (5.3) must hold. Using $j = 0$ in (5.3), we can easily obtain $S_0 = 1$. If $S_\ell = 2^{-\ell}$ for $\ell = 0, \dots, j-1$ with $1 \le j < m-1$, then we deduce from (5.3) that

$$(-2)^j S_j = \delta(j) - \sum_{\ell=0}^{j-1}\frac{j!}{\ell!(j-\ell)!}(-2)^\ell S_\ell = -\sum_{\ell=0}^{j-1}\frac{j!}{\ell!(j-\ell)!}(-1)^\ell = (-1)^j,$$

  from which we must have $S_j = 2^{-j}$. This proves item (2) and we proves (3)⇒(2).

Finally, we prove (2.9). For $\mu = (j_1, j_2)^T \in \mathbb{N}_0^2$ with $|\mu| = j_1 + j_2 < m$, using (5.1) and item (2), we have

$$\begin{aligned}
\sum_{\boldsymbol{k}\in\mathbb{Z}^2} \boldsymbol{a}(\boldsymbol{k})\boldsymbol{k}^\mu &= \sum_{k_1+k_2 \text{ is even}, k_1,k_2\in\mathbb{Z}} \boldsymbol{a}^{2D}(k_1,k_2)k_1^{j_1}k_2^{j_2} + \sum_{k_1+k_2 \text{ is odd}, k_1,k_2\in\mathbb{Z}} \boldsymbol{a}^{2D}(k_1,k_2)k_1^{j_1}k_2^{j_2} \\
&= \frac{1}{2}\sum_{k\in\mathbb{Z}} a^{1D}(k)k^{j_1+j_2} + \frac{1}{2}\sum_{k\in\mathbb{Z}} a^{1D}(k)k^{j_1}(1-k)^{j_2} = \frac{1}{2}S_{j_1+j_2} + \frac{1}{2}\sum_{\ell=0}^{j_2}\frac{j_2!}{\ell!(j_2-\ell)!}(-1)^\ell S_{j_1+\ell} \\
&= 2^{-1-j_1-j_2} + 2^{-1-j_1}\sum_{\ell=0}^{j_2}\frac{j_2!}{\ell!(j_2-\ell)!}(-1)^\ell 2^{-\ell} = 2^{-1-j_1-j_2} + 2^{-1-j_1}(1-2^{-1})^{j_2} = 2^{-j_1-j_2} = 2^{-|\mu|}.
\end{aligned}$$

This proves (2.9). □